IDA PAPER P-2312

CENTRAL RESEARCH PROJECT REPORT ON SUPERCONDUCTIVITY (FY 1988): PART II, MAGNETIC FIELD GRADIOMETER TANK SEEKER

Jeffrey F. Nicoll
Bohdan Balko
Karen K. Garcia

January 1990

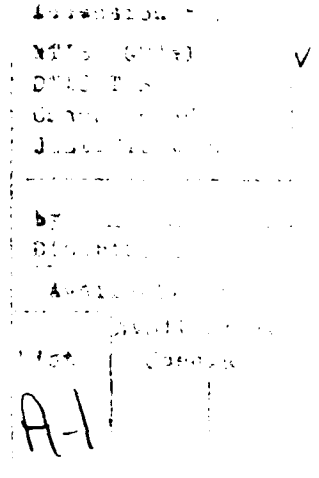

INSTITUTE FOR DEFENSE ANALYSES
1801 N. Beauregard Street, Alexandria, Virginia 22311-1772

DISCLAIMER NOTICE

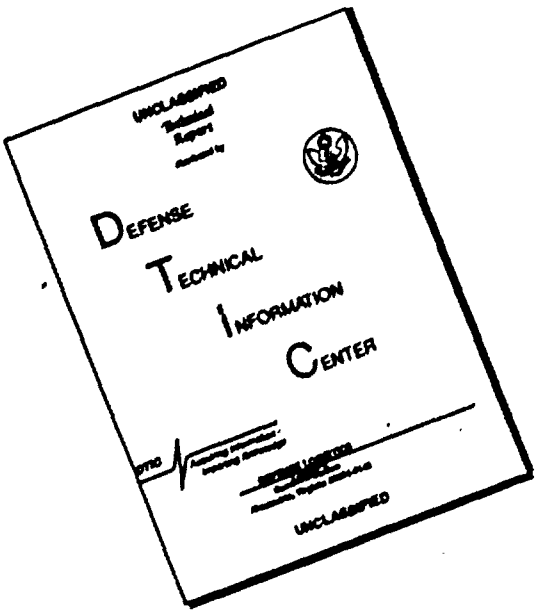

THIS DOCUMENT IS BEST QUALITY AVAILABLE. THE COPY FURNISHED TO DTIC CONTAINED A SIGNIFICANT NUMBER OF PAGES WHICH DO NOT REPRODUCE LEGIBLY.

DEFINITIONS

IDA publishes the following documents to report the results of its work.

Reports

Reports are the most authoritative and most carefully considered products IDA publishes. They normally embody results of major projects which (a) have a direct bearing on decisions affecting major programs, (b) address issues of significant concern to the Executive Branch, the Congress and/or the public, or (c) address issues that have significant economic implications. IDA Reports are reviewed by outside panels of experts to ensure their high quality and relevance to the problems studied, and they are released by the President of IDA.

Group Reports

Group Reports record the findings and results of IDA established working groups and panels composed of senior individuals addressing major issues which otherwise would be the subject of an IDA Report. IDA Group Reports are reviewed by the senior individuals responsible for the project and others as selected by IDA to ensure their high quality and relevance to the problems studied, and are released by the President of IDA.

Papers

Papers, also authoritative and carefully considered products of IDA, address studies that are narrower in scope than those covered in Reports. IDA Papers are reviewed to ensure that they meet the high standards expected of refereed papers in professional journals or formal Agency reports.

Documents

IDA Documents are used for the convenience of the sponsors or the analysts (a) to record substantive work done in quick reaction studies, (b) to record the proceedings of conferences and meetings, (c) to make available preliminary and tentative results of analyses, (d) to record data developed in the course of an investigation, or (e) to forward information that is essentially unanalyzed and unevaluated. The review of IDA Documents is suited to their content and intended use.

The work reported in this publication was conducted under IDA's Independent Research Program. Its publication does not imply endorsement by the Department of Defense, or any other Government agency, nor should the contents be construed as reflecting the official position of any Government agency.

This Paper has been reviewed by IDA to assure that it meets high standards of thoroughness, objectivity, and appropriate analytical methodology and that the results, conclusions and recommendations are properly supported by the material presented.

REPORT DOCUMENTATION PAGE

Form Approved
OMB No. 0704-0188

1. AGENCY USE ONLY *(Leave blank)*	2. REPORT DATE	3. REPORT TYPE AND DATES COVERED
	January 1990	Final--September 1988 to September 1989

4. TITLE AND SUBTITLE

Central Research Project Report on Superconductivity (FY 1988): Part II, Magnetic Field Gradiometer Tank Seeker

5. FUNDING NUMBERS

IDA Independent Research Program

6. AUTHOR(S)

Jeffrey F. Nicoll, Bohdan Balko, Karen K. Garcia

7. PERFORMING ORGANIZATION NAME(S) AND ADDRESS(ES)

Institute for Defense Analyses
1801 N. Beauregard St.
Alexandria, VA 22311-1772

8. PERFORMING ORGANIZATION REPORT NUMBER

IDA Paper P-2312

9. SPONSORING/MONITORING AGENCY NAME(S) AND ADDRESS(ES)

10. SPONSORING/MONITORING AGENCY REPORT NUMBER

11. SUPPLEMENTARY NOTES

12a. DISTRIBUTION/AVAILABILITY STATEMENT

Approved for public release; distribution unlimited.

12b. DISTRIBUTION CODE

13. ABSTRACT ***(Maximum 200 words)***

A feasibility study is described herein for the use of a magnetic field gradiometer SQUID sensor, as a tank seeker and guidance system. It was determined that an antitank missile could be guided by a gradiometer to the target if delivered into a 300-meter bucket with the tank at the center. Problems of ambiguity, multiple targets and decoys, both deliberate and accidental, are discussed with numerical examples.

14. SUBJECT TERMS

High Temperature Superconductivity, SQUID, tank seeker, guidance system, terminal guidance, antitank weapon

15. NUMBER OF PAGES

48

16. PRICE CODE

17. SECURITY CLASSIFICATION OF REPORT	18. SECURITY CLASSIFICATION OF THIS PAGE	19. SECURITY CLASSIFICATION OF ABSTRACT	20. LIMITATION OF ABSTRACT
UNCLASSIFIED	UNCLASSIFIED	UNCLASSIFIED	SAR

IDA PAPER P-2312

CENTRAL RESEARCH PROJECT REPORT ON SUPERCONDUCTIVITY (FY 1988): PART II, MAGNETIC FIELD GRADIOMETER TANK SEEKER

Jeffrey F. Nicoll
Bohdan Balko
Karen K. Garcia

January 1990

INSTITUTE FOR DEFENSE ANALYSES

IDA Independent Research Program

ABSTRACT

A feasibility study is described herein for the use of a magnetic field gradiometer SQUID sensor, as a tank seeker and guidance system. It was determined that an antitank missile could be guided by a gradiometer to the target if delivered into a 300-meter bucket with the tank at the center. Problems of ambiguity, multiple targets and decoys, both deliberate and accidental, are discussed with numerical examples.

CONTENTS

I. INTRODUCTION

By virtue of their high sensitivities, magnetic field sensors employing SQUIDs (Superconductive Quantum Interference Device) have been proposed for a variety of applications (Refs. 1-4). They have been used for such diverse applications as oceanographic and geophysical explorations, medical probing of the human body, in communications, naval warfare, and for radioactive waste location. A particularly useful mode of operating a SQUID is as a magnetic field gradiometer (Ref. 5) which measures to a good approximation a spatial derivative of a component of the magnetic field. Thus, background noise having long spatial correlation lengths (such as the earth's relatively constant magnetic field, for many applications) is automatically suppressed.

If a SQUID gradiometer can be used to locate permanently magnetic or magnetized-by-induction objects it should be capable of seeking, locating, and guiding a missile to such a target. It is the type of application that we are interested in discussing here. *Specifically we are interested in evaluating the possibility of using the SQUID gradiometer as part of a guidance system for an anti-tank weapon.*

Figure 1 illustrates the concept. The superconducting gradiometers inside the missiles sense the magnetic field gradient produced by the tank in the earth's magnetic field. The seeker follows the gradient to the tank and the warhead explodes on contact. The missile has to be directed to within about 150 m from the tank, at which point the gradiometer sensitivity is good enough to guide the missile. One of the benefits of this device is that it could be operated in a shoot-and-forget mode. It could be fired from a great distance as long as it comes to within the 150-m presumed distance or falls into the 150-m radius "bucket" centered on the tank when operated as a mortar. The initial idea for this application was suggested by R. Collins and first described in an IDA report published in 1988 (Ref. 6).

The missile operated with the gradiometer is unaffected by common countermeasures affecting the operation of other devices such as flares, camouflage, decoys, etc. Only large chunks of metal, permanent magnets, or magnetic coils would divert the missile. Thus, it is not generally sensitive to the environment.

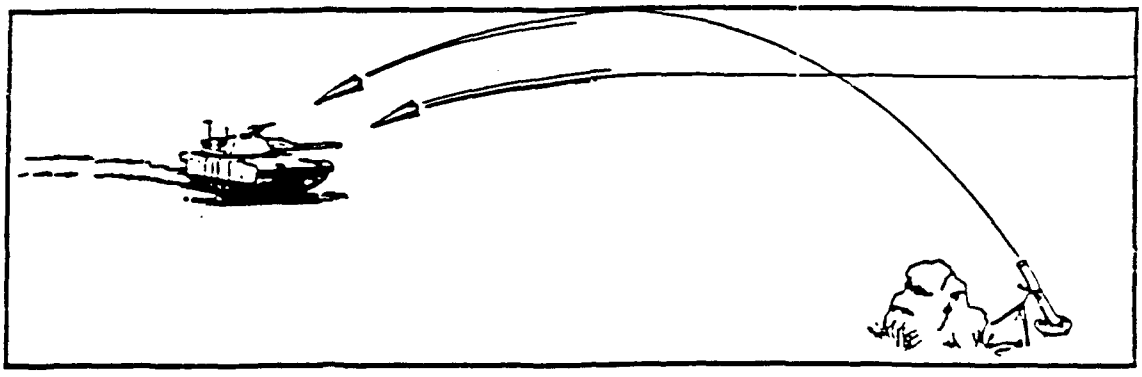

Figure 1. Self-guided Superconducting Probe Weapons Shown Attacking a Tank

II. BACKGROUND

Superconductive magnetic gradiometers have been proposed as detectors of subsurface magnetized materials both in the ground and in the water. One of the advantages of using a gradiometer (as opposed to a magnetometer) is that the gradiometer automatically removes the large constant bias of the geomagnetic field. Also, as noted earlier, large-scale spatial variations in the field (geomagnetic noise) are suppressed, leading to potentially higher operational sensitivities than are possible with a magnetometer. A possible mode of operation for wide area searches of sources of magnetic fields, magnetic anomalies, and electric conductivity anomalies is to place the gradiometer in an airborne vehicle and tow it by an aircraft. In a passive mode such a system could provide large terrain coverage of the distribution of subterranean magnetic anomalies. In an active mode, using both a transmitter and sensor, similar aircraft-towed sensor arrangements have been employed extensively for subsurface conductivity measurements (electromagnetic induction technique) (Refs. 7, 8). A typical system comprises an extra low frequency (ELF) CW (200-4000 Hz) transmitter on the aircraft. The EM fields penetrating the soil are scattered by the spatial conductivity inhomogeneities and are detected by a pickup loop housed in the tethered vehicle.

If a superconducting gradiometer could be made out of the high-temperature superconducting material, it could be employed as a seeker and guidance system for the destruction of tanks on the earth's surface or submarines under the ocean surface. Clearly, a guidance system gradiometer sensor for both applications could be made out of a *low temperature* superconductive material. The added complexity and weight due to the required cryogenics, however, would make the device heavier and much more costly. For the underwater application the extra weight might be tolerable, but for the tank seeker above-ground application this added complexity and weight would make the concept impractical. The two applications are similar conceptually, although the details are different. In this paper we will restrict the discussion to the more demanding and difficult anti-tank application.

Sensitivities quoted in the literature achieved with SQUID gradiometers are on the order of 3×10^{-11}T $m^{-1}Hz^{-1/2}$ or, equivalently, about 10^{-3} $(pT/m)^2/Hz$ (Ref. 8). The

highest sensitivity reported in the literature of 3×10^{-14} Tm^{-1} $Hz^{-1/2}$ was obtained by Wynn et al. (Ref. 9). This intrinsic noise level corresponds to the white noise portion of the spectrum ($f > 0.1$ Hz); at frequencies below about 0.1 Hz the noise power density rises with decreasing frequency, approximately in accordance with the 1/f law. A typical intrinsic noise spectrum achievable with state-of-the-art SQUID gradiometer is shown in Fig. 2.

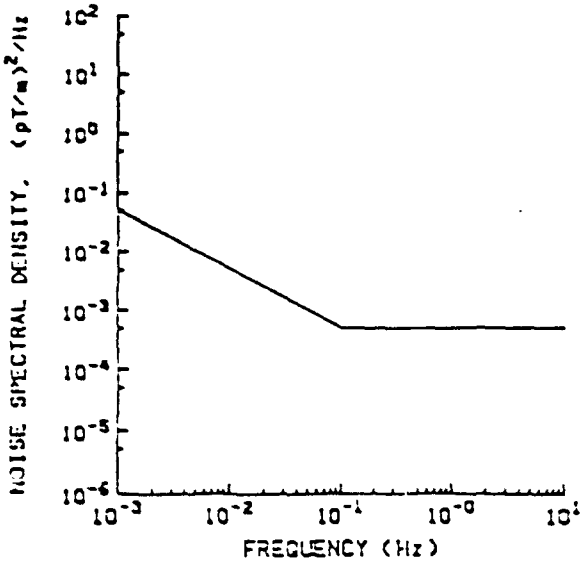

Figure 2. Intrinsic Noise Spectrum of Magnetic Field SQUID Gradiometer

III. TARGET DETECTABILITY

A. SIGNAL STRENGTH AND SENSITIVITY

To determine the plausibility of this detection of tanks in the earth's field we estimate the size of the expected perturbation and compare it to the noise limitations of the SQUID. Considerations of the earth's field are also relevant.

Consider the disruption of the ambient magnetic field, assumed uniform and of magnitude B_0, by a body of magnetic material. If the material is ferromagnetic, there is the possibility that the object will have a permanent magnetic moment. In general, therefore, the exact value of the moment will depend on the precise history of the object (B-H hysteresis) as well as the applied field. For simplicity and as a first estimate, for the lower limit, the effect of hysteresis will be neglected and the object characterized as a linear paramagnetic substance with permeability $\mu >> 1$.

If the object is further taken as an ellipsoid with the applied field parallel to one of the principal axes, then the magnetization, M, is also uniform and parallel to the field. In terms of the demagnetizing factor γ for that axis, M is given by (Ref. 10):

$$4\pi M = \frac{(\mu-1)\, B_o}{(1-\gamma) + \gamma\mu} \quad . \tag{1}$$

For large μ, and $\gamma \neq 0$, the magnetization is essentially independent of the precise value of μ. A long cylinder with the field along its axis has a value of $\gamma = 0$. For a sphere, $\gamma = 1/3$ and all axes are equivalent. For a sphere of radius R, the total magnetic moment, m, is simply the product of the volume, $4\pi R^3/3$, and the magnetization, M, or $m = B_0 R^3$.

The total field is the sum of the applied local field and the dipole field due to the induced magnetization of the "para" or "ferro" magnetic material. A magnetometer can be used to determine the field at any point in space and a gradient magnetometer senses changes in the total field. The limits to determining the field or its spatial derivatives (gradient) is set by the noise in the detector (sensor) systems. Instruments for measuring

the field gradient have been developed over the past decade and superconducting devices have been reported to have limits of the order of 10^{-12} G/cm/Hz$^{1/2}$. This noise limit "S" may have been due to the technology used at the time and is used below for estimation purposes.

For the spherical object described above, the magnitude of the dipole field is

$$B = m/r^3 \quad . \tag{2}$$

where r is the radial distance to the dipole. In this case, the gradient

$$\frac{\partial B}{\partial r} = 3B_o \frac{R^3}{r^4} \quad . \tag{3}$$

This magnitude of the gradient must be compared to the noise "S," that is,

$$\frac{\partial B}{\partial r} > S\,(\Delta f)^{1/2} \quad . \tag{4}$$

In terms of the noise limit, S, the range of detection of a spherical mass is given by

$$r \leq \sqrt[4]{\frac{3\,B_o R^3}{S\,(\Delta f)^{1/2}}} \quad . \tag{5}$$

An estimate of "r" for a typical system is 200 m. Parameters used in this estimate are the mean field of the earth and a sphere of 1-m radius. The mean field of the earth is approximately 0.5 G, a sphere of 1-m radius is approximately 35 tons of iron. A system bandwidth of 100 Hz was taken.

Another, perhaps ultimate, limit is given in terms of flux fluctuations by $S_{flux}^2 = h\,L$, where h is Planck's constant and L is the inductance of the SQUID loop. For

typical loops L = 10^{-9} h, a gradient limit produced by placing two such loops a distance d cm apart is approximately Sd = 8×10^{-14} G/Hz$^{-1/2}$. For d ≈ 10 cm, and a 100-Hz bandwidth, this provides an additional factor of three, or $r_{detection}$ = 600 m. Clearly, it is of great importance to further define the noise limit of such a device.

Use of the dipole gradient makes the range relatively insensitive to changes in the detector. For example, increasing the size of the SQUID loop increases the signal strength proportional to the area of the loop, but increases the noise by the square root of the area. Thus, changing the area of the loops by a factor of 100 only increases S by a factor of 10, and the range by approximately 70 percent.

A more severe limit than the SQUID noise may be the fluctuations in the earth's field. This may provide a more stringent limit than the performance of the SQUIDs.

The simple model offered above suggests several applications, two of which may be of interest to DoD and are described below.

B. MAGNETIC FIELD AND GRADIENT FROM A DIPOLE SOURCE, A COLLECTION OF DIPOLE SOURCES AND AN EXTENDED OBJECT OR MULTIPLE SOURCE

The magnetic field $\vec{B}(\vec{r})$ at point $\vec{r}$ due to a dipole located at the origin, as shown in Fig. 3, is given by:

$$\vec{B}(\vec{r}) = \frac{3\hat{n}\,(\hat{n} \cdot \vec{m}) - \vec{m}}{|\vec{r}|^3}, \tag{6}$$

where $\vec{n}$ is the unit vector pointing in the $\vec{r}$ direction, $\vec{m}$ is the magnetic dipole moment. For the magnetic dipole moment at the origin point in the z direction we have

$$\vec{B}(\vec{X}) = \frac{|\vec{m}|\,(3\hat{n}\cos\theta - \hat{k})}{|\vec{r}|}, \tag{7}$$

where

$$\cos\theta = \frac{z}{|\vec{r}|}, \tag{8}$$

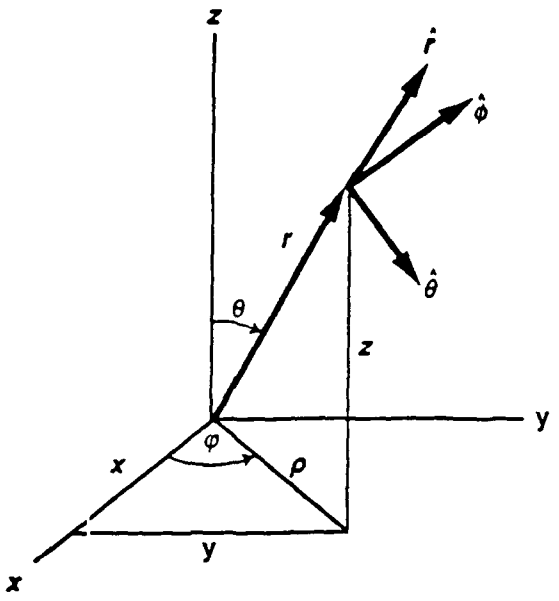

Figure 3. Spherical Coordinate System Used in this Study for Describing a Field as a Function of ρ, θ, φ.

and

$$r = |\vec{r}| = \sqrt{x^2 + y^2 + z^2} \quad . \tag{9}$$

The magnetostatic potential of the total dipole and a constant B_0 field is then given by

$$\Phi = B_o z - K \frac{z}{r^3}, \tag{10}$$

where B_0 is the static field and $K = |\vec{m}|$ is the magnetic dipole moment strength. For spherical objects of radius R_0 of uniform magnetization $K \approx R_o^3 B_o$.

The components of the field

$$B(\vec{X}) = B_x\hat{i} + B_y\hat{j} + B_g\hat{k} \tag{11}$$

are

$$
\begin{aligned}
-\frac{\partial \Phi}{\partial x} &= B_x = 3Kxz\, r^{-5} \\
-\frac{\partial \Phi}{\partial x} &= B_x = 3Kyz\, r^{-5}.
\end{aligned}
\tag{12}
$$

The components of the gradient dyadic

$$
\vec{\vec{Q}} = \begin{pmatrix} Q_{xx} & Q_{xy} & Q_{xz} \\ Q_{yx} & Q_{yy} & Q_{yz} \\ Q_{zx} & Q_{zy} & Q_{zz} \end{pmatrix} , \tag{13}
$$

where

$$
Q_{\alpha\beta} = \frac{\partial}{\partial \beta} B_\alpha \quad , \tag{14}
$$

and the components are given by

$$
\begin{aligned}
Q_{xx} &= 3K(zr^2 - 5x^2z)\, r^{-7} \\
Q_{xy} &= -15Kxyz\, r^{-7} \\
Q_{xz} &= 3K(xr^2 - 5xz)\, r^{-7} \\
Q_{yx} &= -15Kxyz\, r^{-7} \\
Q_{yy} &= 3K(3r^2 - 5y^2z)\, r^{-7} \\
Q_{yz} &= 3K(yr^2 - 5yz^2)\, r^{-7} \\
Q_{zx} &= 3K(-5xz^2 + xr^2)\, r^{-7} \\
Q_{zy} &= 3K(-5yz^2 + yr^2)\, r^{-7} \\
Q_{zz} &= 3K(2zr^2 - 5z^3)\, r^{-7} \quad .
\end{aligned}
\tag{15}
$$

For a collection of N dipoles located at different points r_i and with different dipole strengths k_i we have

$$\Phi = zB_o \sum_{i=1}^{N} K_i \frac{(z - z_i)}{|\vec{r} - \vec{r}_i|^3}$$

$$\vec{B} = \hat{k}\left[B_o - \sum_{i=1}^{N} \frac{K_i}{|\vec{r} - \vec{r}_i|^3} \right] \qquad (16)$$

$$+ 3 \sum_{i=1}^{N} K_i(z - z_i) \frac{(\vec{r} - \vec{r}_i)}{|\vec{r} - \vec{r}_i|^5} \quad .$$

For an extended object, the obvious extension of the above expressions is required.

C. LOCATION OF MAGNETIC OBJECT FROM GRADIOMETER SIGNAL

The purpose of this section is to develop an algorithm, that can be easily implemented on the computer, for locating a magnetic object from a gradient of the magnetic field at a point remote from the object. In subsection (A) we derive an algorithm locating a magnetic dipole (object) in a constant earth's magnetic field. In subsection (B) we develop a procedure for dealing with an extended object whose signature is then described in terms of a multipole expansion.

1. Point Source Magnetic Object in a Constant Field

Consider the magnetic field composed of a uniform field and a dipole oriented with the field; the magnetostatic potential for the far field is given by

$$\phi = B_o z - K \frac{z}{r^3} \quad . \qquad (17)$$

If the field direction is unknown (or if the dipole is not oriented along the field), then the only information available is given by the tensor gradient of the magnetic field:

$$\partial_i \partial_j \phi = \frac{3K}{r^4} M_{ij} \quad , \qquad (18)$$

where the M matrix is given by

$$M_{ij} = \cos\theta\,[\delta_{ij} - 5\,\hat{r}_i\hat{r}_j] + [\hat{r}\,\hat{z} + \hat{z}\,\hat{r}]_{ij} \tag{19}$$

or in other coordinates or in the coordinates shown in Fig. 3.

$$M_{ij} = \cos\theta\,[\delta_{ij} - 3\,\hat{r}_i\hat{r}_j] - \sin\theta\,[\hat{r}\,\hat{\theta} + \hat{\theta}\,\hat{r}]_{ij} \tag{20}$$

where θ is the polar angle from the z axis (the dipole axis). The prefactor of M in Eq. (18) involves the unknown distance and dipole strength of the dipole under consideration and therefore (at least at first) only the relative sizes of the eigenvalues of the matrix are relevant. [For a sphere of permeability μ and radius R_o, $K = (\mu - 1)\,B_o R_o^3/(\mu + 3)$.] Note that M has a simple form if the orientation of the dipole is known; this information is not always available but the procedure below can be simplified if it is known.

M has, in general, three nondegenerate eigenvalues and eigenvectors. The azimuthal direction, ϕ, is always an eigenvector, since it is perpendicular to both the radial and z directions (alternatively to the r and θ directions). Examining the M matrix, it is clear that this eigenvector has eigenvalue

$$\lambda_\phi = \cos\theta\,. \tag{21}$$

The two remaining eigenvalues, corresponding to superpositions of the r and θ directions are solutions of

$$\lambda^2 + \cos\theta\,\lambda - (1 + \cos^2\theta) = 0. \tag{22}$$

The two values straddle the azimuthal eigenvalue

$$\lambda_{\pm} = \frac{-\cos\theta \pm \sqrt{4 + 5\cos^2\theta}}{2} . \qquad (23)$$

[Note that since the prefactor is unknown the eigenvalues of the field gradient tensor will be these values multiplied by $3K/r^4$.] Except for $\cos\theta = \pm 1$, these eigenvalues are nondegenerate. By computing ratios of the three eigenvalues of the gradient tensor, two independent measures can be taken of θ. For example, one can consider the middle eigenvalue divided by the difference of the largest and smallest.

$$\frac{\cos\theta}{\sqrt{4 + 5\cos^2\theta}} = \frac{\lambda_{\text{middle}}}{\lambda_{\text{biggest}} - \lambda_{\text{smallest}}} .$$

Note that the sum of the three eigenvalues must be zero because the magnetic field is divergenceless (this is true for an arbitrary source field, not just the single dipole field); if the measured values do not satisfy this bound, it is a measure of their error. The eigenvectors that correspond to the eigenvalues of Eq. (23) are combinations of the radial and θ directions. Writing the (unnormalized) eigenvectors as

$$\vec{v}_{\pm} = \hat{r} + a_{\pm}\hat{\theta} , \qquad (24)$$

one has the equations

$$\begin{aligned} \lambda_{\pm} &= -2\cos\theta - \sin\theta\, a_{\pm} \\ \lambda_{\pm} a_{\pm} &= -\sin\theta + \cos\theta\, a_{\pm} \end{aligned} \qquad (25)$$

which determines $a_{\pm}$ in terms of the eigenvalues of the M, (or, equivalently, having determined the polar angle θ from the ratio of the eigenvalues the formulas above, in terms of that angle). Note that having determined the polar angle, the value of the prefactor $3K/r^4$ can be determined, which gives an estimate of the range if the rough size of the dipole is

known. Having determined the eigenvectors of M, the radial direction can be recovered by solving the above:

$$\hat{r} = \frac{a_- \vec{v}_+ - a_+ \vec{v}_-}{a_- - a_+} \quad . \tag{26}$$

The procedure for steering is therefore as follows:

- Compute the eigenvalues of the gradient tensor, thereby determining the polar angle.
- Compute the eigenvectors and form the combination given in Eq. (26).
- Estimate the range for a typical size dipole via the prefactor.
- Steer (obviously information from previous time step is useful: Make a Kalman filter!).

Unfortunately, the sign of the eigenvectors is arbitrary so that in the absence of any other information, Eq. (26) gives four possibilities for the radial direction. One can choose the one closest to the direction of motion, or use putative information about the location of the dipole z-axis or location gravitational vertical to disambiguate.

2. Extended Magnetic Object (Point Source Multipole Expansion)

The analytical calculation given for the steering algorithm presumes a single point dipole source for the magnetic field (in addition to any constant background field). The numerical studies of the steering algorithm assumed several additional point dipole sources which could act as decoy targets. Whenever one of these targets is clearly dominant the guidance algorithm is essentially guaranteed to converge on the dominant point dipole. However, real extended sources will have more complex signatures than a simple dipole. As the source is approached, higher multipole contributions to the field will perturb the gradient tensor and at sufficiently short ranges may dominate the dipole contribution. This might lead at short range to a deflected trajectory. This can be explored numerically with extended sources or sets of closely spaced dipole sources. A complete analytic discussion is beyond the scope of the present effort. An initial outline of a multipole perturbation of the steering algorithm will be given in this section.

For an arbitrary scalar potential Φ, the gradient tensor is given by

$$\Phi_{ij} = \hat{\theta}\hat{\theta}\left[\frac{\Phi_r}{r} + \frac{\Phi_{\theta\theta}}{r^2}\right] + \hat{r}\hat{r}\,\Phi_{rr} + \hat{\phi}\hat{\phi}\left[\frac{\Phi_r}{r} + \frac{\Phi_{\theta\theta}}{\sin^2\theta\, r^2} + \frac{\Phi_\theta \cos\theta}{r^2 \sin\theta}\right]$$

$$+\left[\hat{r}\hat{\theta} + \hat{r}\hat{\theta}\right]\left[\Phi_{r\theta} - \frac{\Phi_\theta}{r^2}\right] + \left[\hat{\phi}\hat{r} + \hat{r}\hat{\phi}\right]\left[\frac{\phi_{r\phi}}{r\sin\theta} - \frac{\Phi_\phi}{\sin\theta r^2}\right] \qquad (27)$$

$$+\left[\hat{\phi}\hat{\theta} + \hat{\theta}\hat{\phi}\right]\left[\frac{\Phi_{\phi\theta}}{r^2\sin\theta} - \frac{\cos\theta\,\Phi_\phi}{r^2\sin^2\theta}\right] .$$

The extended source can be represented in the "far" field by an expansion in spherical harmonics.

$$\phi = \frac{1\, P_1(\cos\theta)}{3\, r^2} + \sum_{lm} a_{lm}\, \frac{Y_{lm}(\theta,\phi)}{3r^{l+1}} \qquad (28)$$

where the 1/3 is introduced to match the prefactors used earlier.

One may imagine considering the effect of a single Y_{lm} term on the steering in the following way. The gradient tensor can be computed with the dipole and perturbational term included. The eigenvectors and eigenvalues can be computed and the operations of the steering algorithm given previously applied to the new situation. The error in the assignment can then be computed as a function of the a_{lm} coefficient. To first order in perturbation theory these effects may be summed. The algebra needed for this program is tedious but not difficult and will be pursued in later work. For current purposes, only a few general remarks need be made.

First, the vanishing of the divergence of the magentic field is equivalent to the vanishing of the trace of the gradient tensor (equivalently, the eigenvalues sum to zero). This condition holds for any multipole expansion as can be verified by direct examination of the equivalent partial differential equation for Φ.

Second, in the dipole-only case considered earlier, the largest and smallest eigenvectors are contained in the r-θ plane. Thus, the operations given above are equivalent to determining the angle through which the largest and smallest eigenvectors (which are orthogonal) must be rotated to align them with the r-θ directions. For the multipole expansion case with $m = 0$ (no explicit ϕ dependence) this property is preserved. The effect of the higher order multipoles is to change the required angle of rotation but the radial direction still lies in the plane spanned by the largest and smallest eigenvectors. (For infinitesimal perturbations, the relative size of the eigenvectors is unchanged whenever there are three distinct eigenvalues.) For $m \neq 0$, this does not hold and the true radial direction will lie out of the plane of the largest and smallest eigenvectors.

The algebra for even the simplest example of $m = 0$, $1 = 2$ (quadrapole) case does not appear to be immediately enlightening and will not be reproduced here. Progress in the multipole expansion requires either a long series of calculations to be done by hand or the use of a symbolic manipulation program such as MACSYMA.

IV. STEERING CODE DEVELOPMENT AND TESTING

A. BACKGROUND

Using the theoretical basis laid down in Section II we developed a code which is designed to utilize gradiometer measurements to steer a missile. In this section we describe the code and examine its capabilities. The code, which we will refer to as XGRAP inverts the gradiometer signal to obtain a direction which points to the source of the field. It turns out that such an inversion is not unique but produces, in general, four vectors, two pointing in the directions of the source or more accurately into the hemisphere in which the source is located and the two others point into the opposite hemisphere. These latter two can be dispensed with easily on grounds that the missile knows the difference between forward and backward directions.

Clearly, to develop a code which can be used in the field to guide missiles requires many steps including:

1. Test of mathematical validity of the code under simulated operational conditions, assuming pure signal (no noise or decoys).
2. Determination of the effects of noise both natural and manmade.
3. Determination of the effect on results of false targets, including decoys.
4. Determination of the effect on steering of ambiguous signals (i.e., missile equidistant from two targets.
5. Determination of the range of operation of system.
6. Simulation of all relevant physical processes, including flight characteristics, acceleration, steering response, etc.

In this paper we touch on all of the above points with the exception of (6). From the examples to be presented here it will become clear that more in-depth analysis is required to determine the realistic bounds of operability of the proposed steering system. The intent here is to show feasibility rather than to attempt to conduct an exhaustive study of special cases.

B. PROGRAM XGRAP--ALGORITHM STRUCTURE

The following steps are taken in the code to steer the missile in a course toward the magnetic source.

Step 1. Calculations of the magnetic field gradient $\overrightarrow{\overrightarrow{Q}}$ at the missile position x_o, y_o, z_o. This is stored as a matrix

$$\overrightarrow{\overrightarrow{Q}}(x_o, Y_o, z_o) = \begin{pmatrix} Q_{xx} & Q_{xy} & Q_{xz} \\ Q_{yx} & Q_{yy} & Q_{yz} \\ Q_{zx} & Q_{zy} & Q_{yz} \end{pmatrix} \tag{29}$$

Step 2. Calculations of the eigenvalues and eigenfunction of $\overrightarrow{\overrightarrow{Q}}$ x_o, y_o, z_o as shown below.

Eigenvalues	Order	Eigenvectors
λ_+	high	$\overrightarrow{v}_+$
λ_-	least	$\overrightarrow{v}_-$
λ_o	middle	$\overrightarrow{v}_o$

Step 3. Calculation of $\cos\theta$ from equation

$$\frac{\cos\theta}{4 + 5\cos^2\theta} = \frac{\lambda_o}{\lambda_+ - \lambda_-} \tag{30}$$

and a check on the eigenvalues to see if

$$\lambda_+ + \lambda_- + \lambda_o = 0. \tag{31}$$

Step 4. Description of eigenvectors in terms of angular unit vectors so that

$$\vec{v}_+ = \hat{r} + a_+ \hat{\theta}$$
$$\vec{v}_- = \hat{r} + a_- \hat{\theta} \tag{32}$$

and a+, a- are determined from

$$\lambda_+ = -2\cos\theta - \sin\theta\, a_+$$
$$\lambda_- = -2\cos\theta - \sin\theta\, a_- \tag{33}$$

Two checks are made at this point to determine if

$$\lambda_\pm a_\pm = -\sin\theta + \cos\theta\, a_\pm \tag{34}$$

and

$$|v_\pm|^2 = 1 + a_\pm^2 \tag{35}$$

Step 5. Determination of the direction of the target $\vec{R}_T$ by

$$\vec{R}_T = \frac{a - \vec{v}_+ - a_+ \vec{v}_-}{a_- - a_+} \tag{36}$$

Step 6. The missile is moved from point x_0, y_0, z_0 to point y_1, y_1, z_1 in the direction $\vec{R}_T$, at which time the process of following steps 1 through 5 is repeated and a new point x_2, y_2, z is reached. The process is depicted in Fig. 4.

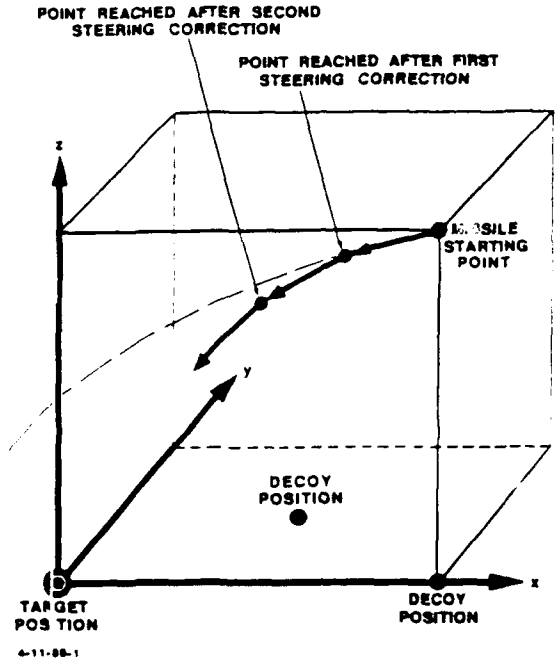

Figure 4. Illustration of the Steering Process

C. TESTING OF CODE XGRAP

In preparation for the steering algorithm tests we made a study of the field $\vec{B}$ and field gradient $\overrightarrow{\overrightarrow{Q}}$ resulting from different magnetic dipole distributions as shown in Fig. 5. The following four figures (Figs. A-1 through Fig. A-4) show some sample field and gradient distributions. In these figures a grid of $10 \times 10 \times 10$ points is used and the field vector and gradient matrix were calculated at each point. In each case considered, a cut is taken through the y-axis at y = 1 and the values of the fields at the 100 points in the (x, y = 1, z) plane are shown.

The basic format of the figures is as follows: the top three views in each figure (a, b, c) show the equal magnetic field contour lines of the components B_x, B_y, B_z, respectively. The next six views (d, e, f, g, h, i) show the equal magnetic field gradient contour lines Q_{xx}, Q_{yy}, Q_{zz}, Q_{xy}, Q_{xz}, Q_{yz}, respectively. The other components are redundant because of symmetry. In each figure the logarithm of the value is actually plotted.

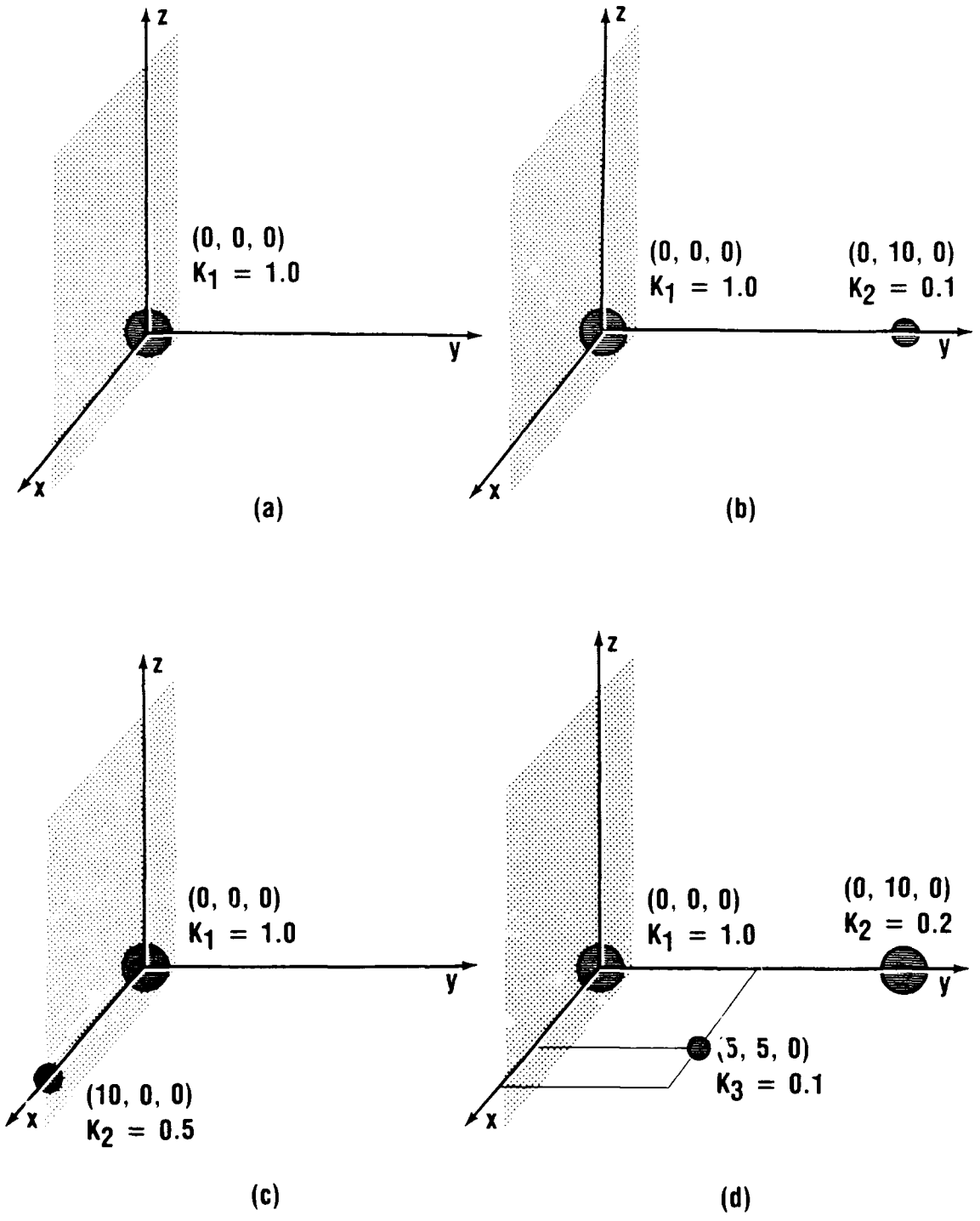

Figure 5. Location of Different Magnetic Dipoles as Used in the Magnetic Field and Gradient Contour Plots in Figs. 6 Through 16.

Table 1 shows the location of the components in Figs. A-1 through A-4.

Table 1. Location of Magnetic Field and Gradient Components In Figs. A-1 through A-4.

B_x	B_y	B_z
Q_{xx}	Q_{yy}	Q_{zz}
Q_{xy}	Q_{xy}	Q_{yz}

Figure 5 shows the location and relative strengths of the dipoles used in the subsequent calculations. The plane (x, y = 1, z) is also indicated by shading. In Fig. A-1 the contour plots for fields resulting from a single dipole of strength 1.0 located at (0, 0, 0) are shown. In Fig. A-2, in addition to the dipole at (0, 0, 0) of strength 1.0, another dipole of strength 0.1 is assumed located at (0, 10, 0). In Fig. A-3, the second dipole is moved to (10, 0, 0) and its strength is increased to 0.5. To calculate the results shown in the last figure of this series, Fig. A-4, three dipoles are assumed. The first dipole of strength 1.0 is at (0, 0, 0) the second is at (0, 10, 0) and has a strength of 0.2 and the third is located at (5, 5, 0) and has a relative dipole strength of 0.1.

It is difficult to determine the effect on the steering algorithm from such plots. The decision was made to just use the algorithm in specific situations and see what happens.

The steering algorithm GRAMPS was tested for several dipole distributions with different dipole strengths K_i located at points (x_i, y_i, $z_i = 0$). A $10 \times 10 \times 10$ grid was used. The missile was assumed to be flying at a predetermined constant velocity v_M and at time t = 0 to be located at point ($x_0 = 10$, $y_0 = 10$, $z_0 = 10$). The gradient matrix $\overrightarrow{\overrightarrow{Q}}$ was calculated at this point as described in Section II with GRAD and the inverse operation was performed with code GRAMPS. One of the two resultant vectors pointing in the forward hemisphere was selected and the missile moved in this direction for time period Δt to point (x_1, y_1, z_1). At this point the process was repeated and another direction selected corresponding to the previous vector found at point (x_0, y_0, z_0). This process was repeated until the missile either hit or missed the target. Table 2 gives the dipole strengths

Table 2. Dipole Strength and Location Used for the Calculations Shown In Figs. A-5 through A-13

Dipole Strengths	Dipole Location (x, y, z)	Results Shown in Figure No.
1.0	(0, 0, 0)	A-5
1.0 0.1	(0, 0, 0) (10, 0, 0)	A-6
1.0 0.5	(0, 0, 0) (10, 0, 0)	A-7
1.0 0.1	(0, 0, 0) (0, 10, 0)	A-8
1.0 0.2	(0, 0, 0) (0, 10, 0)	A-9
1.0 0.1 0.1	(0, 0, 0) (0, 10, 0) (5, 5, 0)	A-10
1.0 0.2 0.1	(0, 0, 0) (0, 10, 0) (5, 5, 0)	A-11
1.0 0.1 0.2	(0, 0, 0) (0, 10, 0) (5, 5, 0)	A-12
1.0 0.2 0.2	(0, 0, 0) (0, 10, 0) (5, 5, 0)	A-13

and locations used in a number of steering calculations and Figs. A-5 through A-15 show the results of the calculations. In each figure, drawing (a) shows the initial vectors indicated by $\vec{a}$, $\vec{b}$, a', and b', and drawings (b) and (c) show paths taken as guided by the algorithm GRAMPS. Note that although a symmetric situation was selected setting initial conditions for the run shown in Fig. A-14, the algorithm still guides the missile to a target. By symmetry consideration one might expect the missile to be guided between the targets. It seems, however, that a slight numerical error breaks the symmetry and prevents this

from happening. In a real situation in the field we expect that this would also occur and that slight perturbations in the fields would break the symmetry and force the missile to one of the two targets.

Our limited sample shows that:

1. The steering algorithm works when the target is isolated from decoys. When decoys are present, the steering algorithm can be misled as shown in Fig. 10(c) and (d). In this case the decoy of strength $K_2 = 10$ was 10 units away from the starting point or $\frac{\sqrt{2}}{2}$ times closer than the target. Since the dipole field goes like $\frac{1}{(\text{distance})^3}$ this means that the interaction between target and sensor and decoy and sensor is in the ratio of $\frac{\sqrt{2}}{4}$. The decoy has a stronger attraction for the target.
2. Either of the vectors $\vec{a}$ or $\vec{b}$ pointing in the forward hemisphere will direct or steer the missile to the desired target.
3. It seems that the size of the angle between the vectors from the inverse solution may be a good indication of the steering effectiveness. If the two vectors that point in the forward direction subtend on angle < 90 deg the steering will be successful. If this angle is > 90 deg a false target will be reached.

Clearly, further analysis is required. The present results only point the ways to more simulations and analysis. These results, however, do indicate feasibility of steering by using the gradiometer measurements.

V. COUNTERMEASURES

The magnetic SQUID gradiometer tank seeker could be overcome by

1. Building tanks out of a nonmagnetic alloy,
2. Reducing the signature of magnetized tanks (deperming and degaussing) below a measurable level,
3. Introducing false signatures,
4. Providing decoys to simulate the tank's magnetic signature and divert the seeker.

As far as we know there are no tanks constructed solely from nonmagnetic material, and it is not likely that this can be done in the foreseeable future. Ceramic armor is being used, but other components of a tank are not built completely out of ceramic or non-magnetic material.

Degaussing and deperming are well developed procedures used by the Navy to protect surface ships and submarines from mines. Deperming removes some of the permanent magnetization of the vessel produced during material processing and manufacture. The effect lasts for about two years, at which point the process can be repeated. Degaussing has to be performed continuously because it removes the induced field due to the earth's field. This has to be done on demand and has to be customized to the earth's field conditions.

Degaussing with coils on a surface vessel can be accomplished easily down to 20 percent of the induced magnetization (vertical component). With a lot more effort, a reduction down to 5 percent is predicted. For submarines, degaussing is not practiced because of the weight of coils and power requirements. Deperming is more practical and is used for both surface vessels and submarines.

For tanks, no operational system for reducing the magnetic signature by degaussing or deperming exists. This technology has been evaluated and a deperming cage constructed for test purposes. Reduction down to 20 percent of original value has been obtained. Clearly, this number could be improved, but the cost and operational utility has to be established. The Army seems to be more interested in signature modification designed to

trigger mines well ahead of tanks than in signature reduction. A lot of work has gone into this effort. How well these signature modification techniques and signal reduction techniques will actually work in the field to countermeasure the seeker has to be determined through tests, evaluation, and further analysis.

Other possible countermeasures include the use of permanent or electromagnets used as "flares" to distract the seeker. For the permanent magnet, it is simple to compute the required size of the decoy.

Assume that the decoy is made from a magnetic material with a permanent magnetization M ($B = 4\pi M$). The dipole moment of such a decoy is independent of the details of the shape of the object and is given by the product of M and the volume. This can be seen by the following example. Consider a cylinder with cross-sectional area A, and length L, with the magnetization M oriented along the cylinder axis. This is equivalent for purposes of calculating the external field, to a surface current (in cgs units) $K = cM$. The dipole moment is given by $m = IA/c = KLA/c = MAL = M$ Volume. In general, the dipole moment of the material is given by $m = \int M\, dV = M$ Volume.

The dipole moment of the target was estimated (conservatively) as $m_{target} = B_0R^3$, with R taken as 1 m. For a permanent magnet decoy, $m_{decoy} > m_{target}$) or $M_{decoy} V_{decoy} > B_0R^3$. For Swedish iron, an inexpensive magnetic material, $M \approx 10^3$ corresponding to $B \sim 12{,}000$ gauss. Since $B_0R^3$is approximately unity, $V_{decoy} \approx 10^{-3}$ $m^3 = 10^3$ cm^3 (1 liter). Each of these decoys would therefore weigh about 8 kg. These would have to be discharged at roughly 100-m intervals to be effective as decoys. In 10 km, about a ton of decoys would be needed. More exotic material may raise M by an order of magnitude (decreasing the volume by the same amount), but would increase the cost.

This is close to the absolute limit to be expected if all the (relevant) spins in the material were aligned. The magnetic moment per spin is $eh/4\pi mc = 0.93 \times 10^{-20}$ gauss-cm^3. As an order of magnitude estimate, one may take two spins per atom and 10^{23} atoms/cm^3, this yields $M_{limit} \approx 1.8 \times 10^3$. Therefore, no material is likely to extend this limit significantly. The use of an electromagnet is unlikely to improve the values; an air core magnet will have a lower field than one with a permeable core, and these will be subject to the same limits as the permanent magnets.

VI. SUMMARY AND CONCLUSIONS

We have looked at the feasibility of using a squid gradiometer as a sensor for an antitank missile terminal guidance system. It is well known that inversion of the gradiometer signal (from a collection of magnetic dipoles) gives an ambiguous result for the direction of the target; four vectors in pairs pointing in opposite directions. For this reason the determination of the magnetic gradient in general would not be a very useful measurement for a tank detection and guidance system, without additional information.

In our application, some additional information is available and two directions can be selected from the four derived vectors. It turns out that both vectors lead to the target by different routes when our algorithm is applied. We have performed simulations of missile guidance assuming various target and decoy magnetic strengths and spatial distributions. How well the algorithm works depends on the relative signal strengths and distances to missile of the target and decoy. Several representative situations have been investigated.

We also estimated the range of application of the SQUID gradiometer system. For an isolated tank with only an induced moment due to the earth's field, the approximate distance from the target at which a SQUID gradiometer can begin to guide the missile is 150 m. Thus, for the guidance system to be effective, the missile nas to be shot into a "bucket" 300 m in diameter with the target in the center.

Our results show that the principle of inverting a gradiometer signal to obtain guidance for a missile designed to attach a magnetic target is sound. Whether the system can be made practical depends on the feasibility of building a SQUID from high temperature superconductive material with low noise characteristics at temperatures high enough so that lightweight refrigeration is possible. Since work on SQUIDS is going on now, the answers to these questions are forthcoming.

After questions regarding SQUID characteristics and refrigeration requirements are resolved, questions regarding missile dynamics have to be addressed. Clearly, the missile speed and maneuverability have to be designed around the sensor. We do not expect that

the sensor could be merely adapted to an existing missile. Finally, the question of countermeasures has been addressed, but further in-depth work in this area has to be initiated.

REFERENCES

1. W. Podney and R. Sager, "Measurement of Fluctuating Magnetic Gradients Originating From Oceanic Internal Waves," *Science*, Vol. 205, pp. 1381-1382, September 1979.

2. W. Podney and R. Sager, *Measurement of Fluctuating Magnetic Gradients Over Coastal Waters*, Physical Dynamics, Inc., La Jolla, California, March 1980.

3. T.G. Gamble, W.M. Goubau, and John Clarke, *Magnetolellurics With a Remote Magnetic Reference*, Lawrence Berkeley Laboratory Report LBL-7032, January 1978.

4. J.E. Zimmerman and W.H. Campbell, "Tests of Cryogenic SQUID for Geomagnetic Field Measurements," *Geophysics*, Vol. 40, No. 2, pp. 269-284, April 1975.

5. M.B. Ketchen, W.M. Goubau, and J. Clarke, "Superconducting Thin-Film Gradiometer," *J. Appl. Phys.* **49**(7), pp. 4111-4116, July 1978.

6. B. Balko, L. Cohen, R. Collins, J. Hove, J.F. Nicoll, "Central Research Project Report on Superconductivity (FY 1987)," IDA Memorandum Report M-468, May 1988.

7. F.S. Grant and G.F. West, *Interpretation Theory in Applied Geophysics*, McGraw Hill Book Co., 1965.

8. *Mining Geophysics, Vol. II*, The SEG Mining Geophysics Volume Editorial Committee, D.A. Houser, et al., Assoc. Eds., published by the Society of Exploration Geophysicists, Tulsa, Oklahoma, 1966.

9. W.M. Wynn, C.P. Frahm, P.J. Carroll, R.H. Clark, J. Wellhoner, and W.J. Wynn, *IEEE Trans. Magn.*, MAG-11 701, 1975.

10. T.D. Jackson, *Classical Electrodynamics*, John Wiley & Sons, Inc., New York, 1962.

APPENDIX

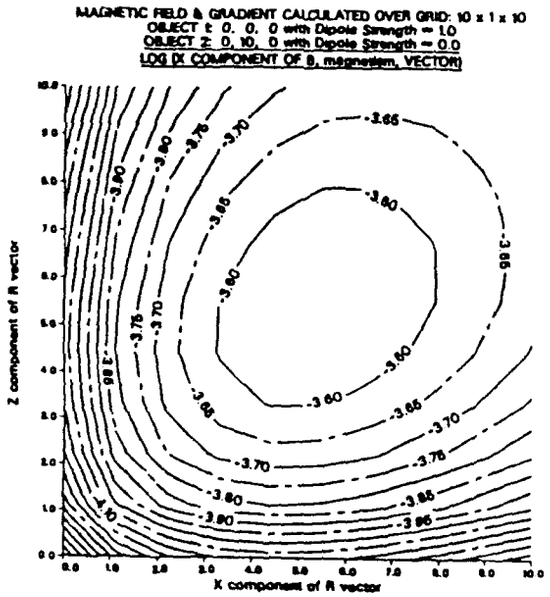
MAGNETIC FIELD & GRADIENT CALCULATED OVER GRID: 10 x 1 x 10
OBJECT 1: 0, 0, 0 with Dipole Strength = 1.0
OBJECT 2: 0, 10, 0 with Dipole Strength = 0.0
LOG (X COMPONENT OF B, magnetism, VECTOR)
Z component of R vector
X component of R vector

(a)

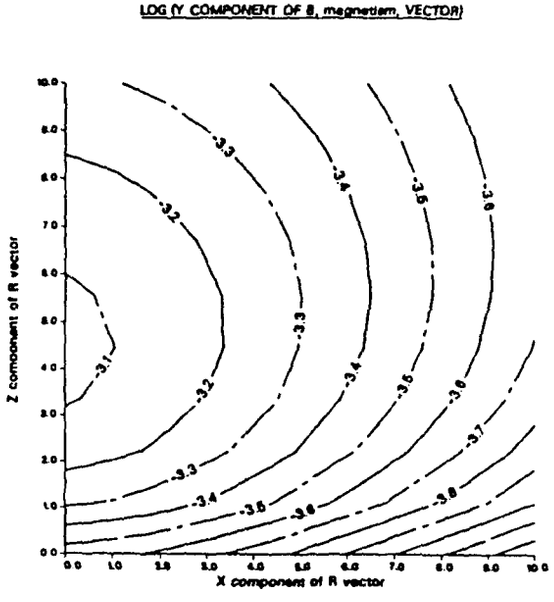
LOG (Y COMPONENT OF B, magnetism, VECTOR)
Z component of R vector
X component of R vector

(b)

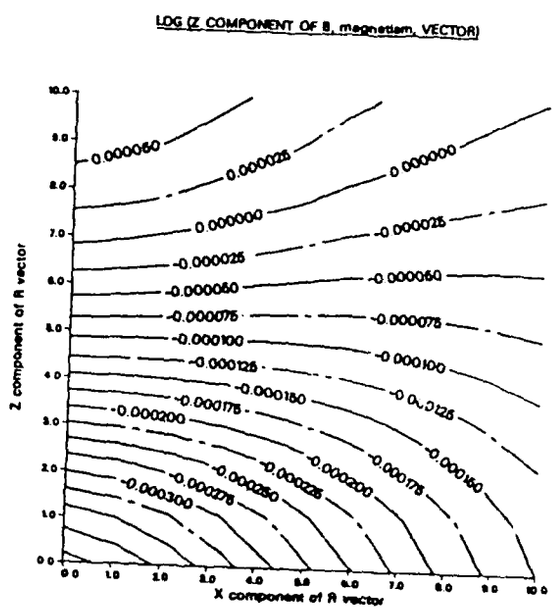
LOG (Z COMPONENT OF B, magnetism, VECTOR)
Z component of R vector
X component of R vector

(c)

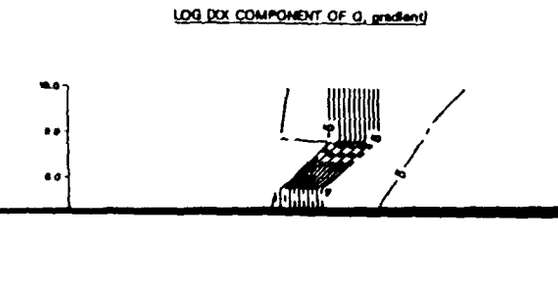
LOG (XX COMPONENT OF G, gradient)

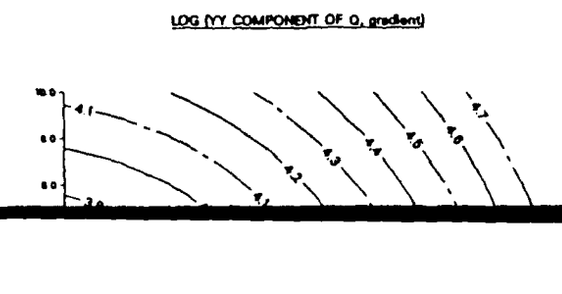
LOG (YY COMPONENT OF G, gradient)

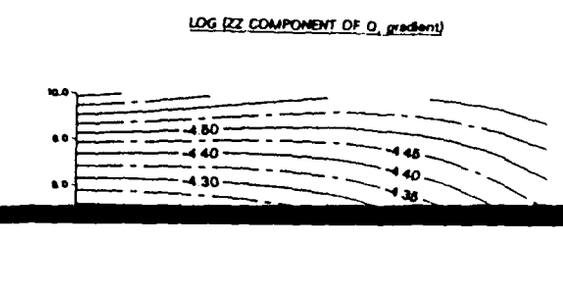
LOG (ZZ COMPONENT OF G, gradient)

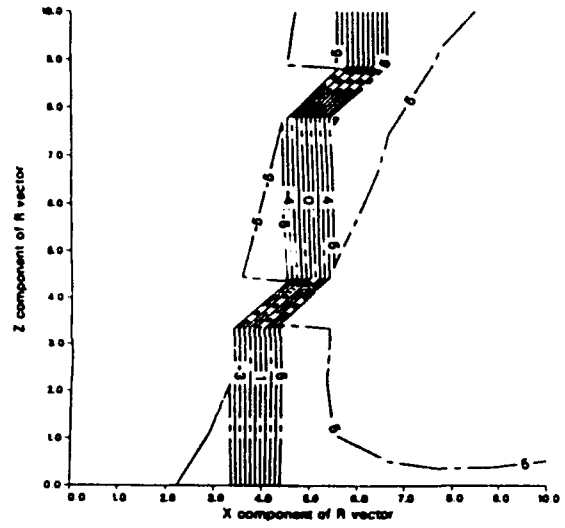

(d)

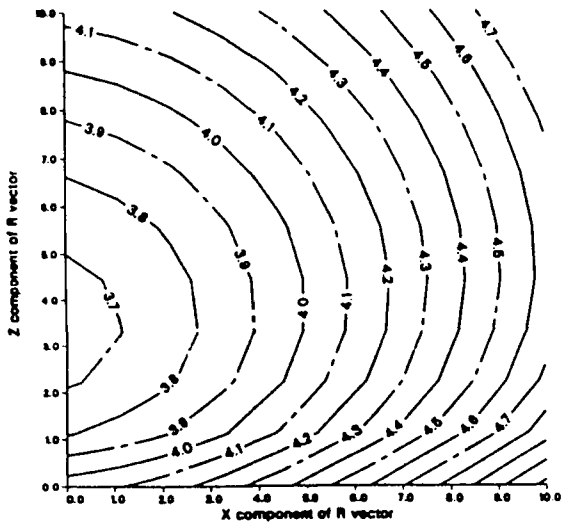

(e)

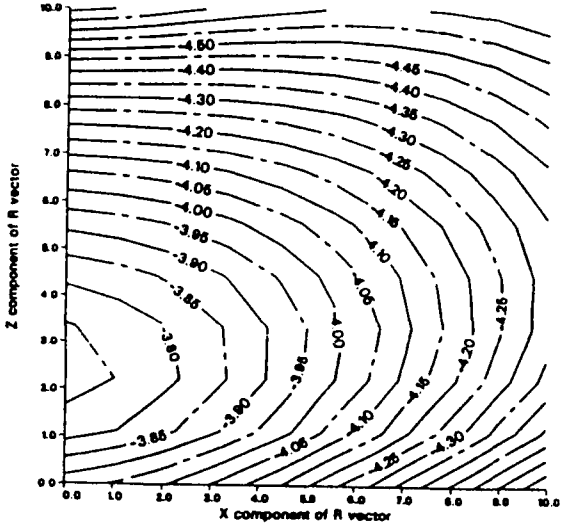

(f)

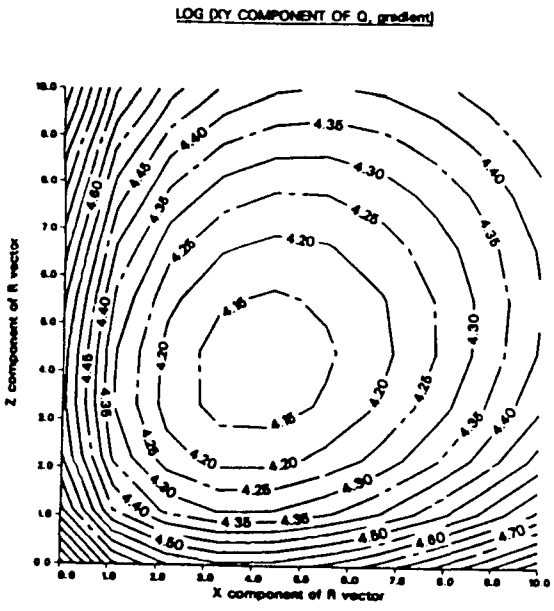

(g)

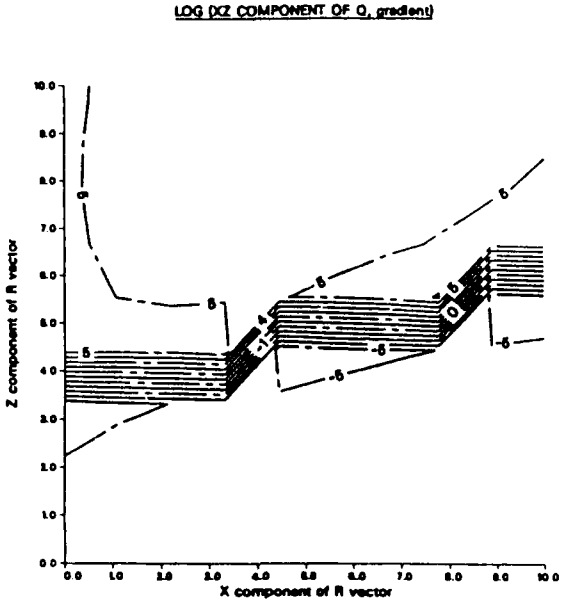

(h)

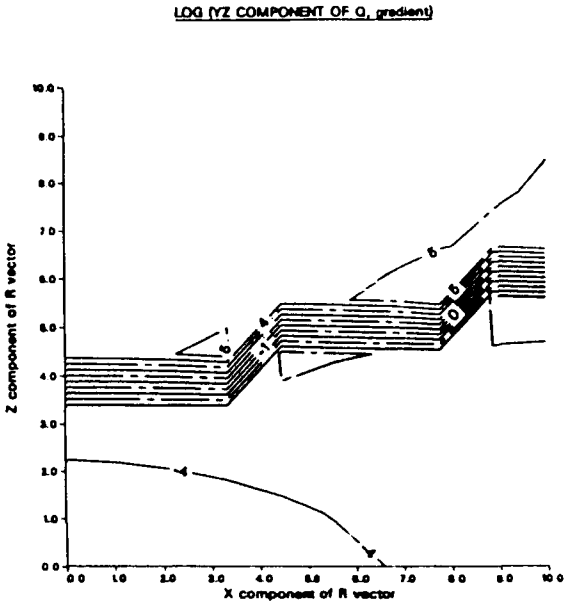

(i)

Figure A-1. Distributed Dipole Field Study. Contour plots of magnetic field components [(as), (b), (c)] and magnetic field gradient components [(d), (e), (f), (g), (h), (i)], plotted in the x, I, z) plane. Dipole located at (0,0,0) of strength 1.0.

MAGNETIC FIELD & GRADIENT CALCULATED OVER GRID: 10 x 1 x 10
OBJECT 1: 0, 0, 0 with Dipole Strength = 1.0
OBJECT 2: 0, 10, 0 with Dipole Strength = 0.1
LOG (X COMPONENT OF B, magnetism, VECTOR)

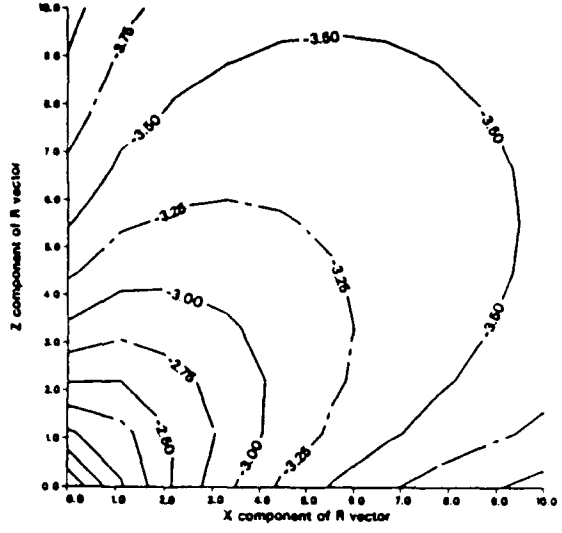

(a)

LOG (Y COMPONENT OF B, magnetism, VECTOR)

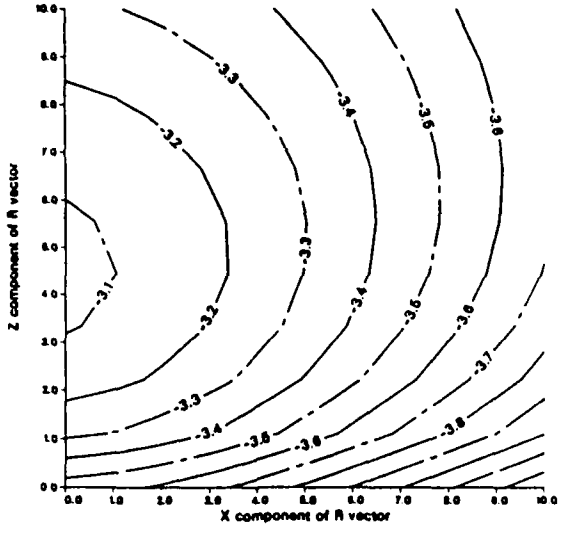

(b)

LOG (Z COMPONENT OF B, magnetism, VECTOR)

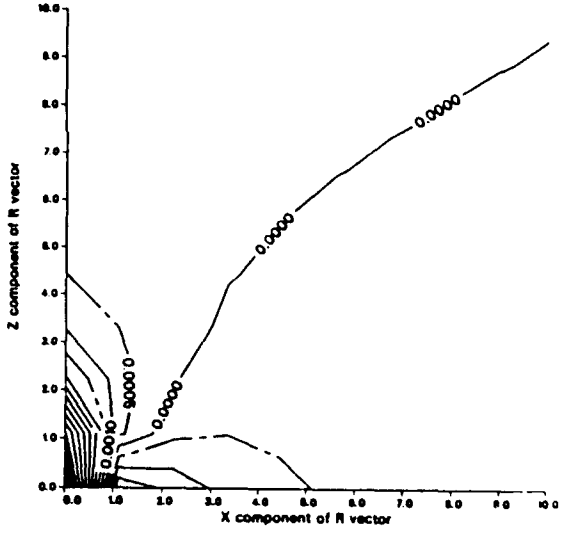

(c)

LOG (XX COMPONENT OF Q, gradient)

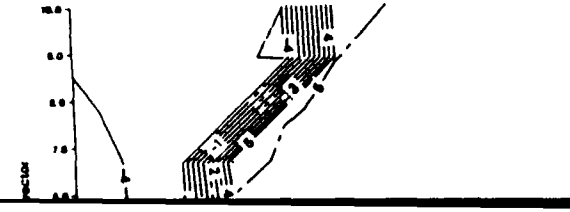

LOG (YY COMPONENT OF Q, gradient)

LOG (ZZ COMPONENT OF Q, gradient)

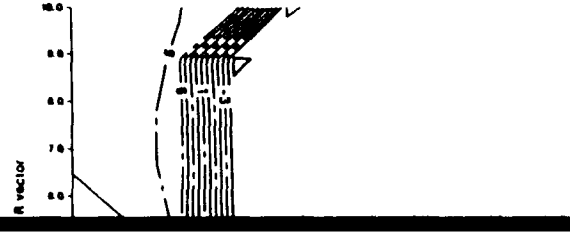

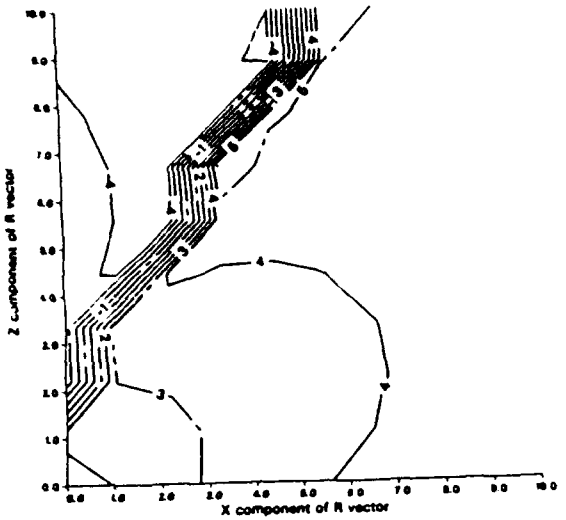

(d)

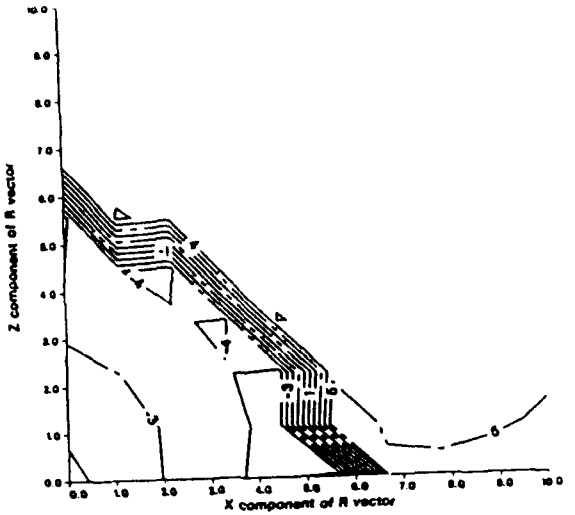

(e)

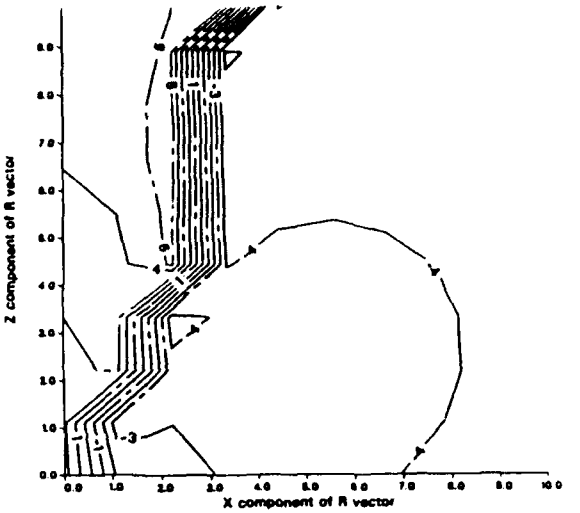

(f)

LOG (XY COMPONENT OF Q, gradient)

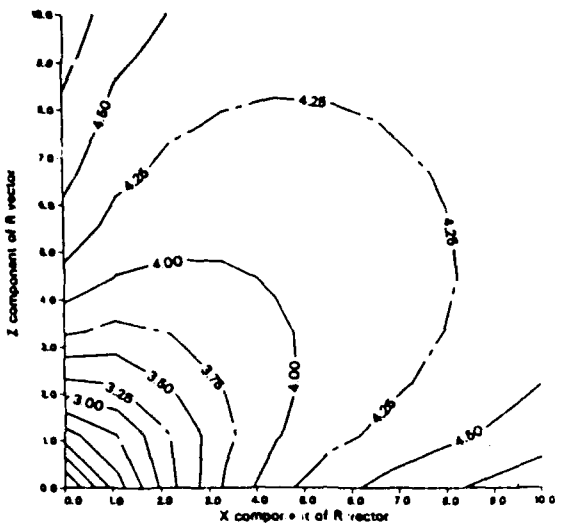

(g)

LOG (XZ COMPONENT OF Q, gradient)

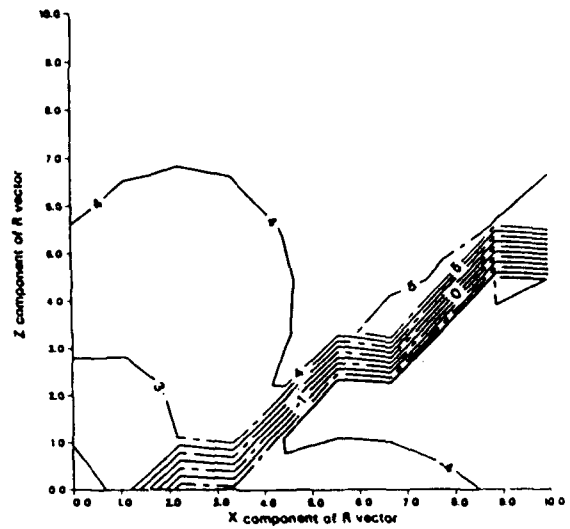

(h)

LOG (ZY COMPONENT OF Q, gradient)

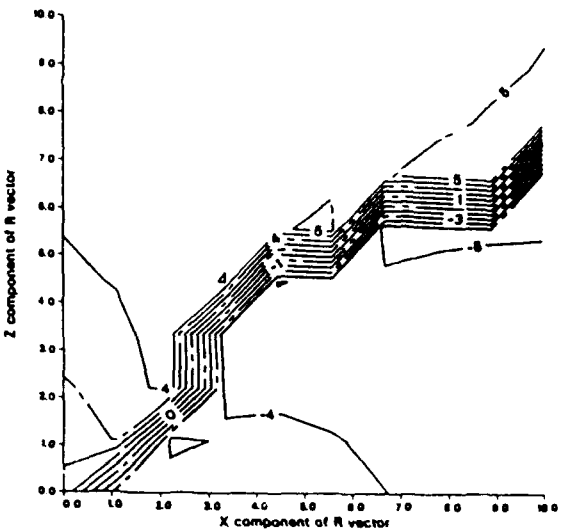

(i)

Figure A-2. Distributed Dipole Field Study. Contour plots of magnetic field components [(as), (b), (c)] and magnetic field gradient components [(d), (e), (f), (g), (h), (i)], plotted in the x, I, z) plane. Dipoles located at (0,0,0) and (0,10,0) of strengths 1.0 and 0.1, respectively.

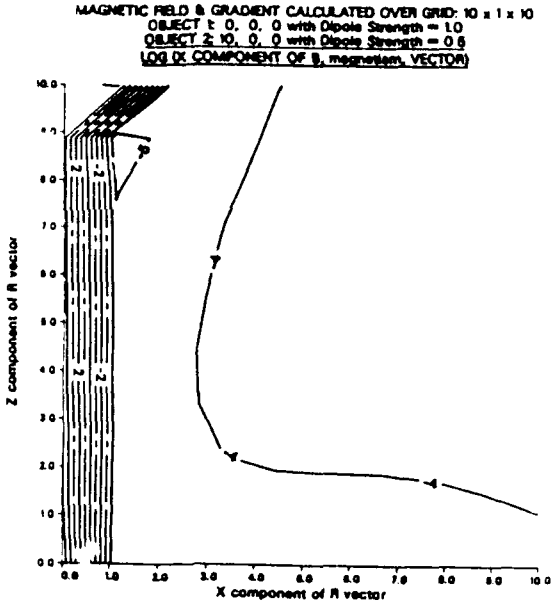
MAGNETIC FIELD & GRADIENT CALCULATED OVER GRID: 10 x 1 x 10
OBJECT 1: 0, 0, 0 with Dipole Strength = 1.0
OBJECT 2: 10, 0, 0 with Dipole Strength = 0.6
LOG (X COMPONENT OF B, magnetism, VECTOR)
Z component of R vector
X component of R vector

(a)

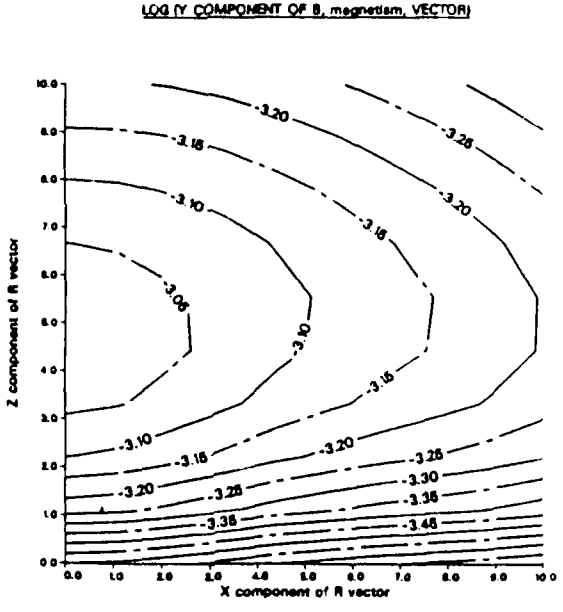
LOG (Y COMPONENT OF B, magnetism, VECTOR)
-3.20
-3.15
-3.10
-3.05
-3.25
-3.30
-3.35
-3.40
-3.45
Z component of R vector
X component of R vector

(b)

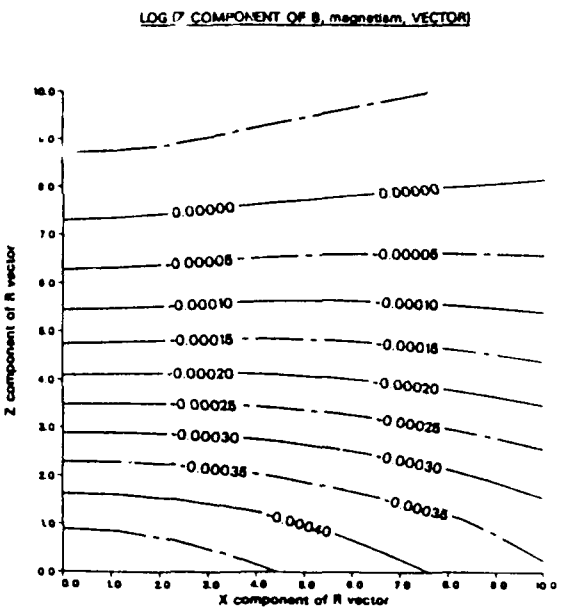
LOG (Z COMPONENT OF B, magnetism, VECTOR)
0.00000
-0.00005
-0.00010
-0.00015
-0.00020
-0.00025
-0.00030
-0.00035
-0.00040
Z component of R vector
X component of R vector

(c)

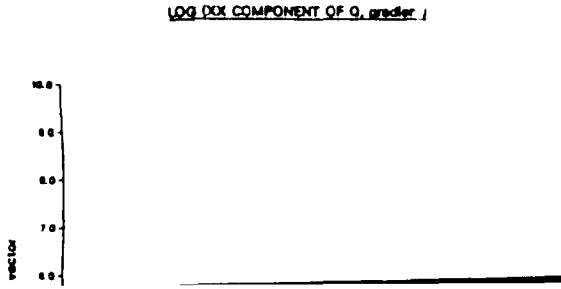
LOG (XX COMPONENT OF Q, gradient)
Z component of R vector

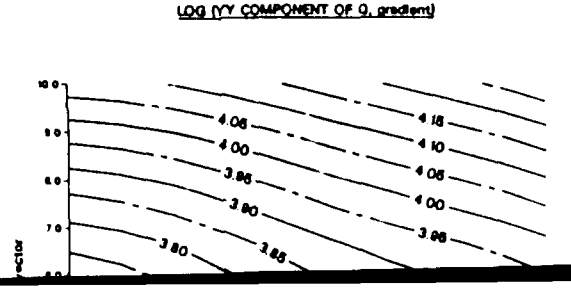
LOG (YY COMPONENT OF Q, gradient)
4.05
4.00
3.95
3.90
3.85
3.80
4.15
4.10
4.05
4.00
3.95

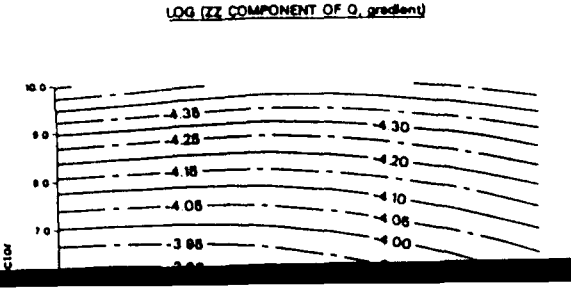
LOG (ZZ COMPONENT OF Q, gradient)
-4.35
-4.25
-4.15
-4.05
-3.95
-4.30
-4.20
-4.10
-4.06
-4.00

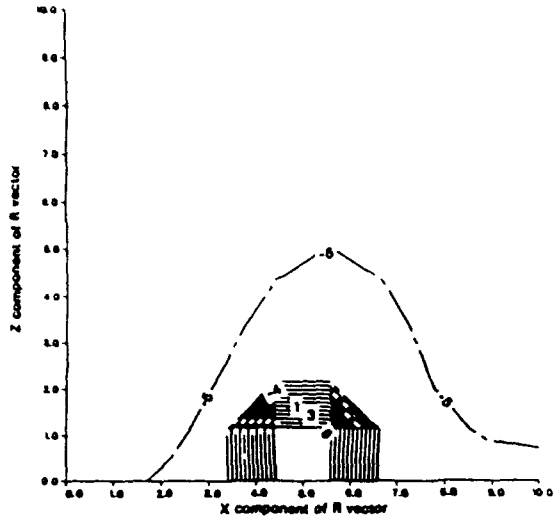

(d)

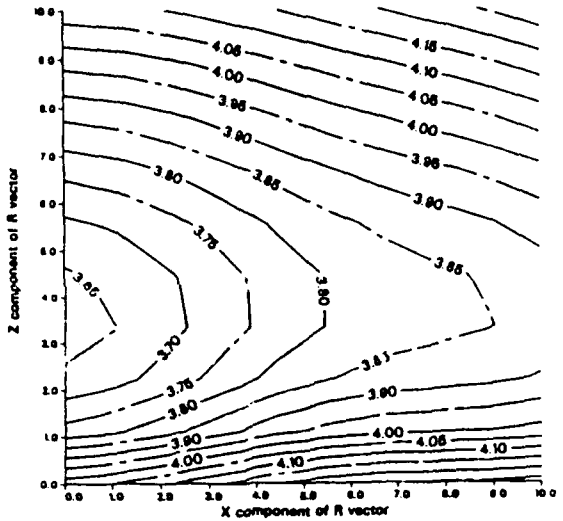

(e)

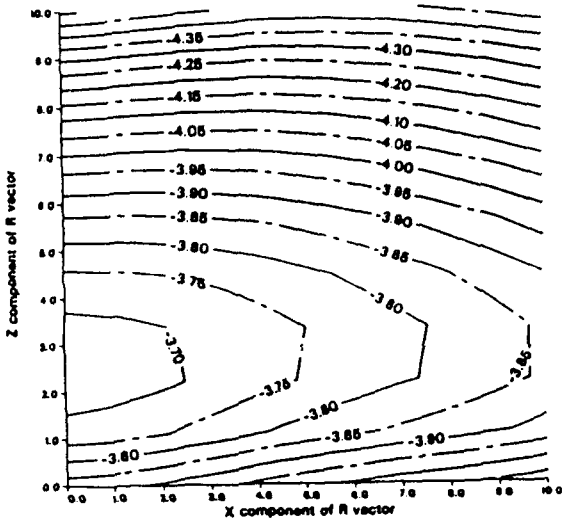

(f)

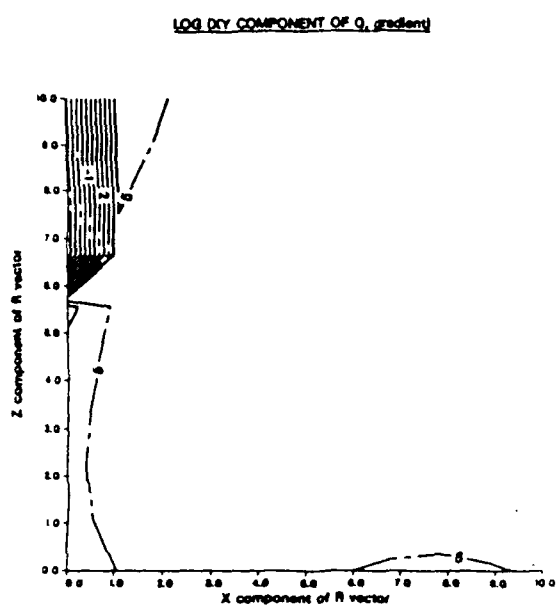

(g)

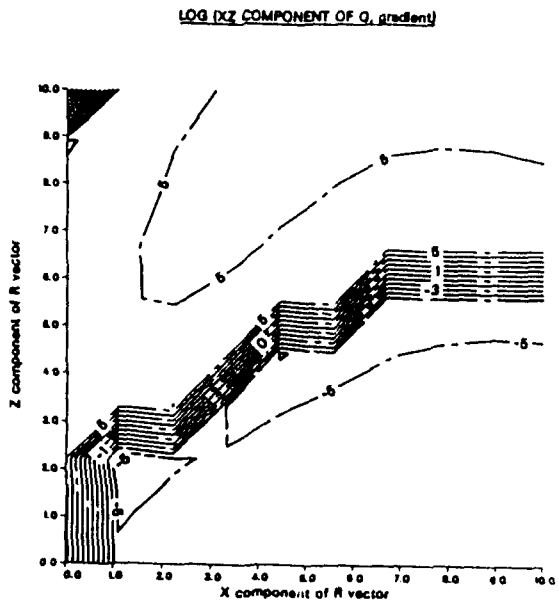

(h)

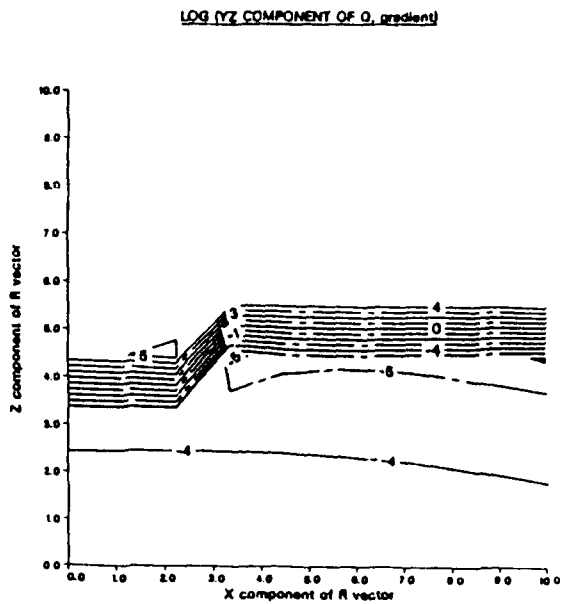

(i)

Figure A-3. Distributed Dipole Field Study. Contour plots of magnetic field components [(as), (b), (c)] and magnetic field gradient components [(d), (e), (f), (g), (h), (i)], plotted in the x, I, z) plane. Dipoles located at (0,0,0) and (10,0,0) of strengths 1.0 and 0.5, respectively.

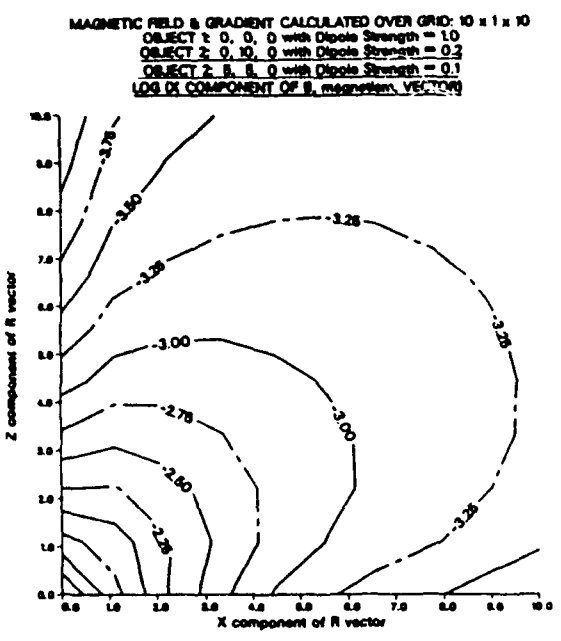
MAGNETIC FIELD & GRADIENT CALCULATED OVER GRID: 10 x 1 x 10
OBJECT 1: 0, 0, 0 with Dipole Strength = 1.0
OBJECT 2: 0, 10, 0 with Dipole Strength = 0.2
OBJECT 2: 8, 8, 0 with Dipole Strength = 0.1
LOG (X COMPONENT OF B, magnetism, VECTOR)
Z component of R vector
X component of R vector
-3.75
-3.50
-3.25
-3.00
-2.75
-2.50
-2.25

(a)

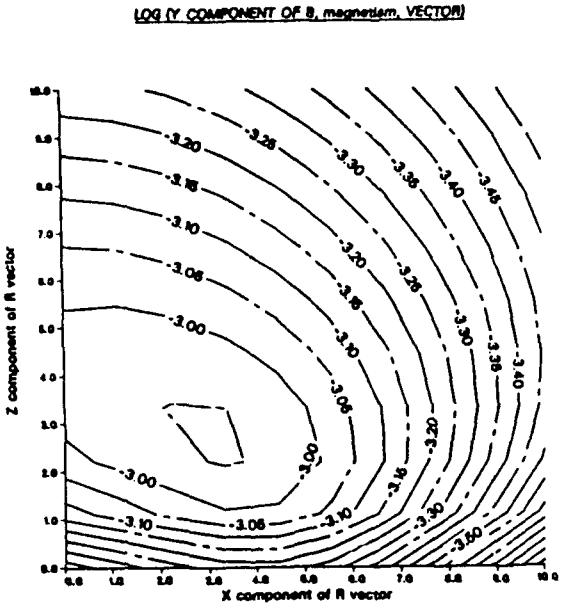
LOG (Y COMPONENT OF B, magnetism, VECTOR)
Z component of R vector
X component of R vector
-3.20
-3.25
-3.30
-3.35
-3.40
-3.45
-3.15
-3.10
-3.05
-3.00

(b)

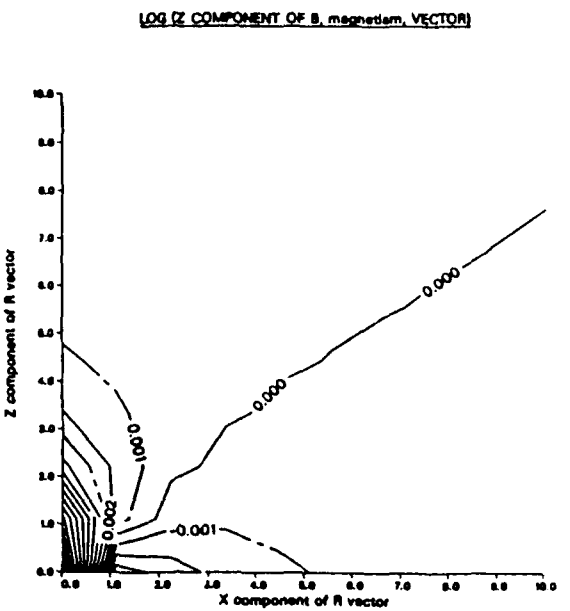
LOG (Z COMPONENT OF B, magnetism, VECTOR)
Z component of R vector
X component of R vector
0.000
0.000
0.001
0.002
-0.001

(c)

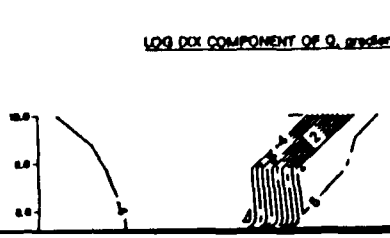
LOG (XX COMPONENT OF Q, gradient)

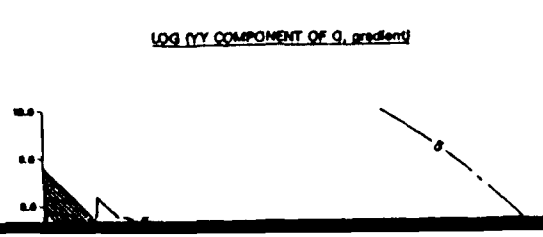
LOG (YY COMPONENT OF Q, gradient)

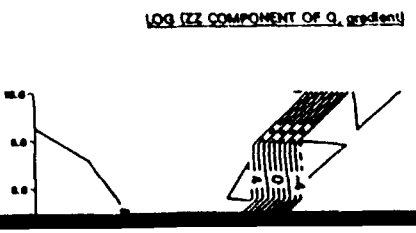
LOG (ZZ COMPONENT OF Q, gradient)

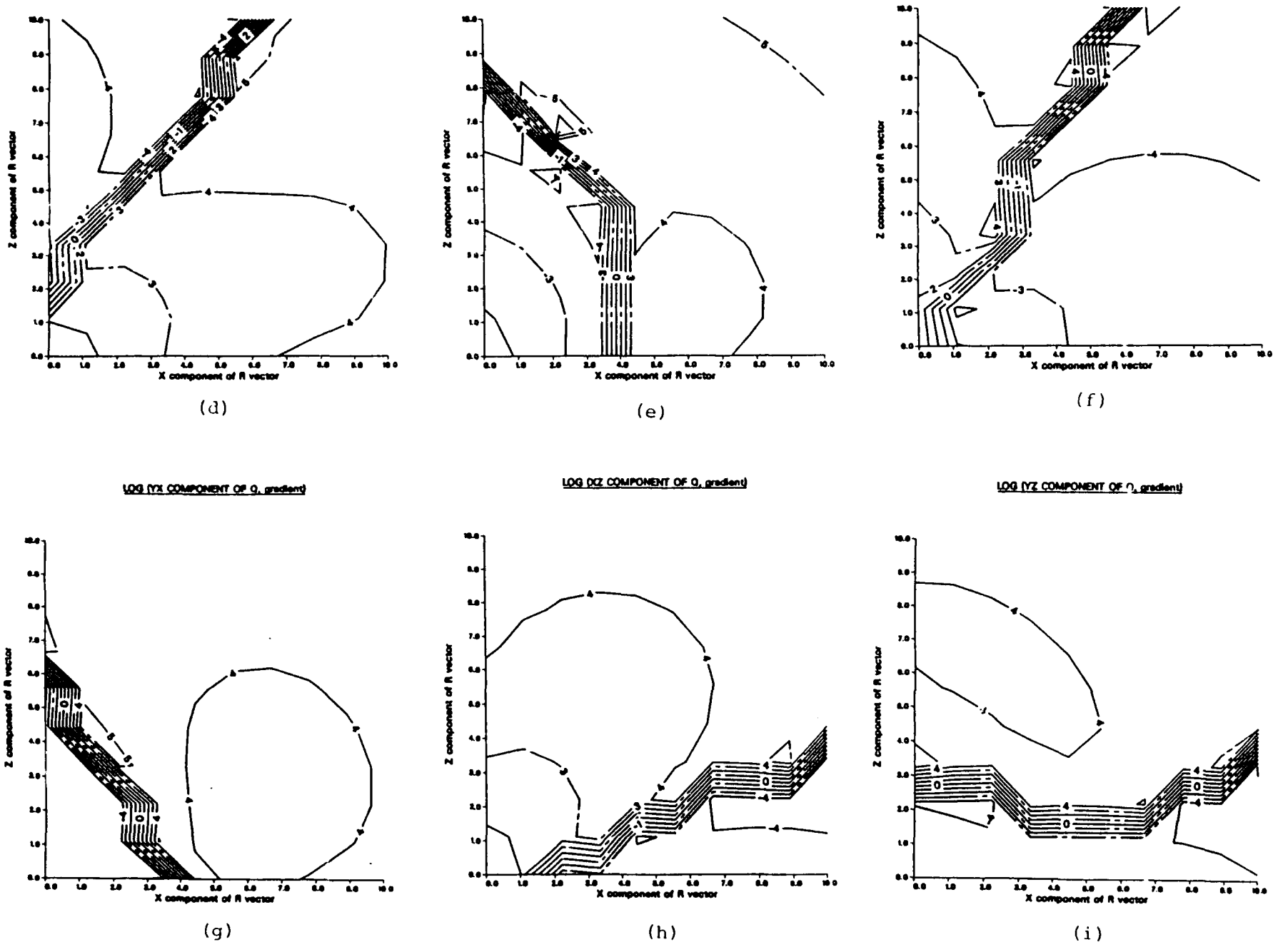

Figure A-4. Distributed Dipole Field Study. Contour plots of magnetic field components [(as), (b), (c)] and magnetic field gradient components [(d), (e), (f), (g), (h), (I)], plotted in the x, I, z) plane. Dipoles located at (0,0,0), (0,10,0) and (5,5,0) of strengths 1.0, 0.5, and 0.1, respectively.

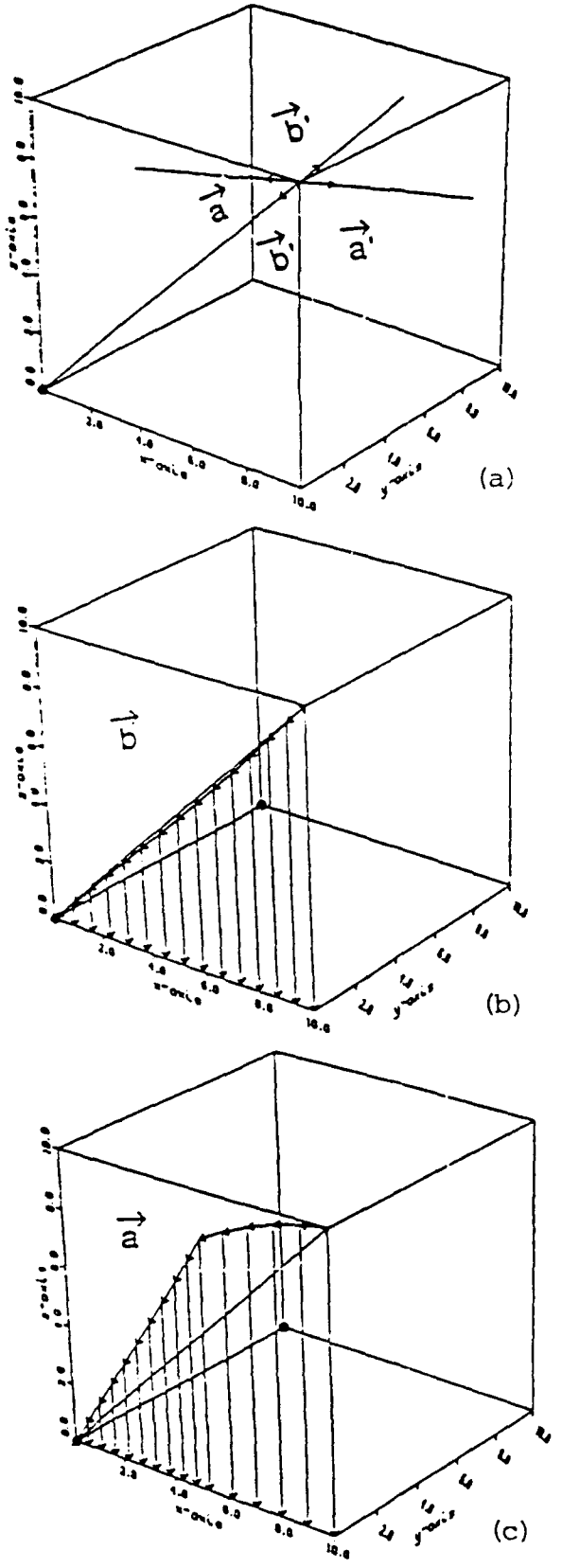

Figure A-5. Simulation of steering by gradiometer initial conditions with derived vectors $\vec{a}$, $\vec{b}$, $\vec{a}'$ and $\vec{b}'$ are shown in (a), and missile trajectories following vectors $\vec{a}$ and $\vec{b}$ are shown in (b) and (c). A magnetic dipole of strength K = 1.0 is assumed to be located at (0,0,0) in this calculation.

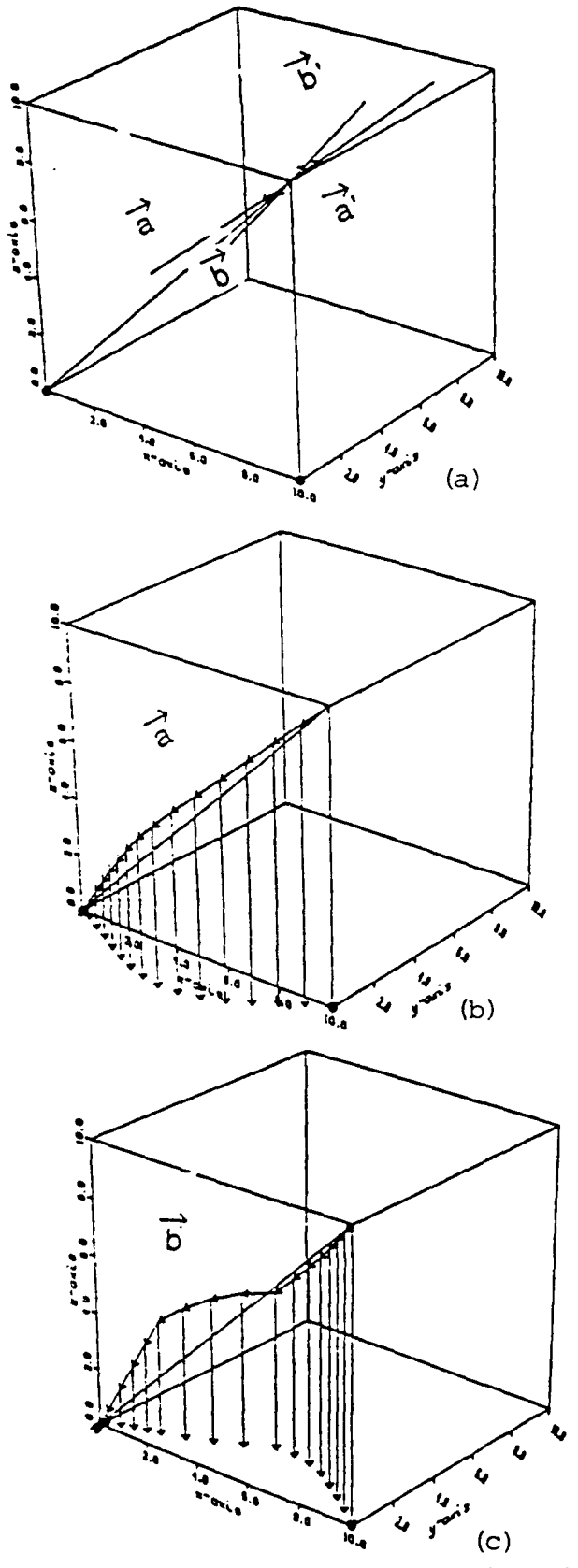

Figure A-6. Simulation of steering by gradiometer initial conditions with derived vectors $\vec{a}$, $\vec{b}$, $\vec{a}'$ and $\vec{b}'$ are shown in (a), and missile trajectories following vectors $\vec{a}$ and $\vec{b}$ are shown in (b) and (c). Magnetic dipoles of strengths K_1 = 1.0 and K_2 = 0.1 are assumed to be located at point (0,0,0) and (10,0,0), respectively.

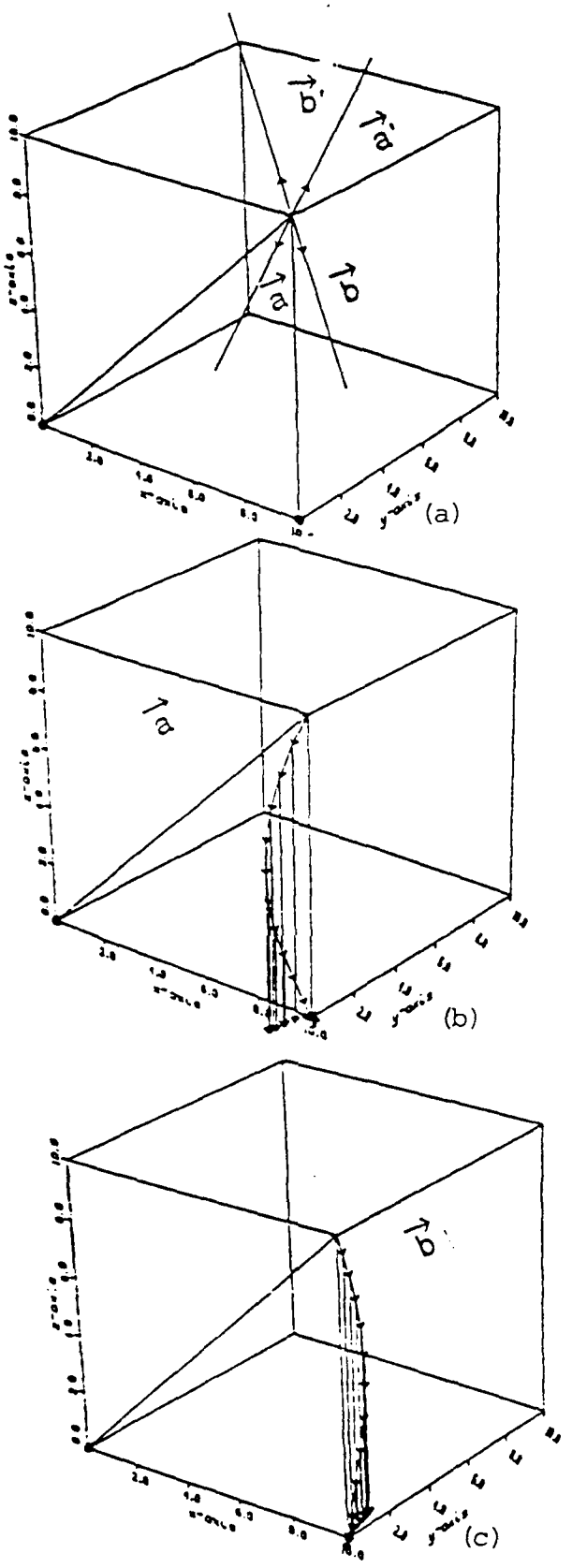

Figure A-7. Simulation of steering by gradiometer initial conditions with derived vectors $\vec{a}$, $\vec{b}$, $\vec{a}'$ and $\vec{b}'$ are shown in (a), and missile trajectories following vectors $\vec{a}$ and $\vec{b}$ are shown in (b) and (c). Magnetic dipoles of strengths K_1 = 1.0 and K_2 = 0.5 are assumed to be located at point (0,0,0) and (10,0,0), respectively.

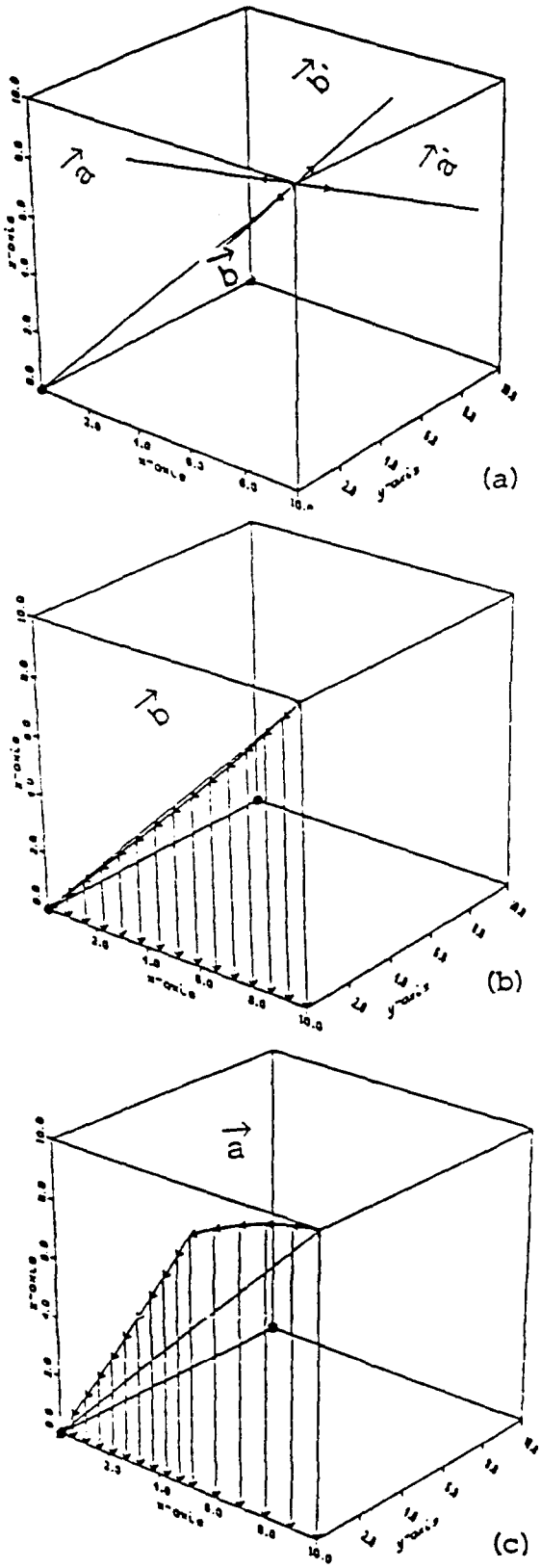

Figure A-8. Simulation of steering by gradiometer initial conditions with derived vectors $\vec{a}$, $\vec{b}$, $\vec{a}'$ and $\vec{b}'$ are shown in (a), and missile trajectories following vectors $\vec{a}$ and $\vec{b}$ are shown in (b) and (c). Magnetic dipoles of strengths K_1 = 1.0 and K_2 = 0.1 are assumed to be located at point (0,0,0) and (0,10,0), respectively.

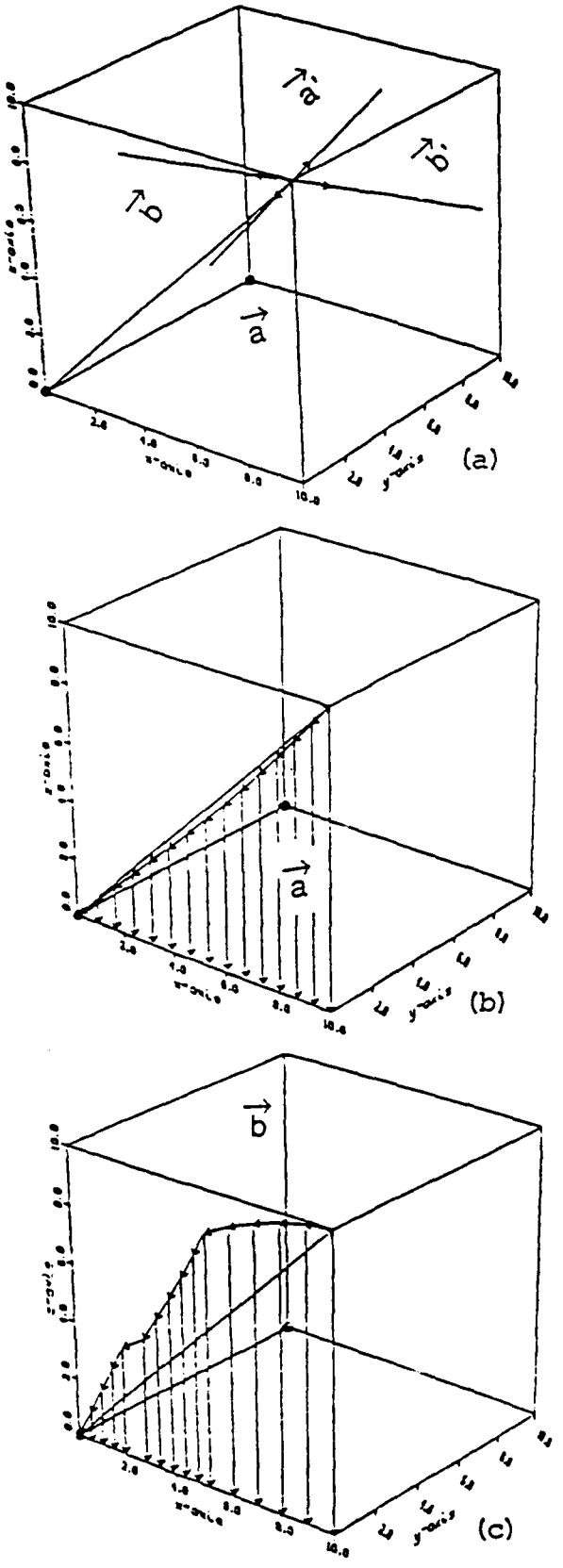

Figure A-9. Simulation of steering by gradiometer initial conditions with derived vectors $\vec{a}$, $\vec{b}$, $\vec{a}'$ and $\vec{b}'$ are shown in (a), and missile trajectories following vectors $\vec{a}$ and $\vec{b}$ are shown in (b) and (c). Magnetic dipoles of strengths K_1 = 1.0 and K_2 = -0.2 are assumed to be located at point (0,0,0) and (0,10,0), respectively.

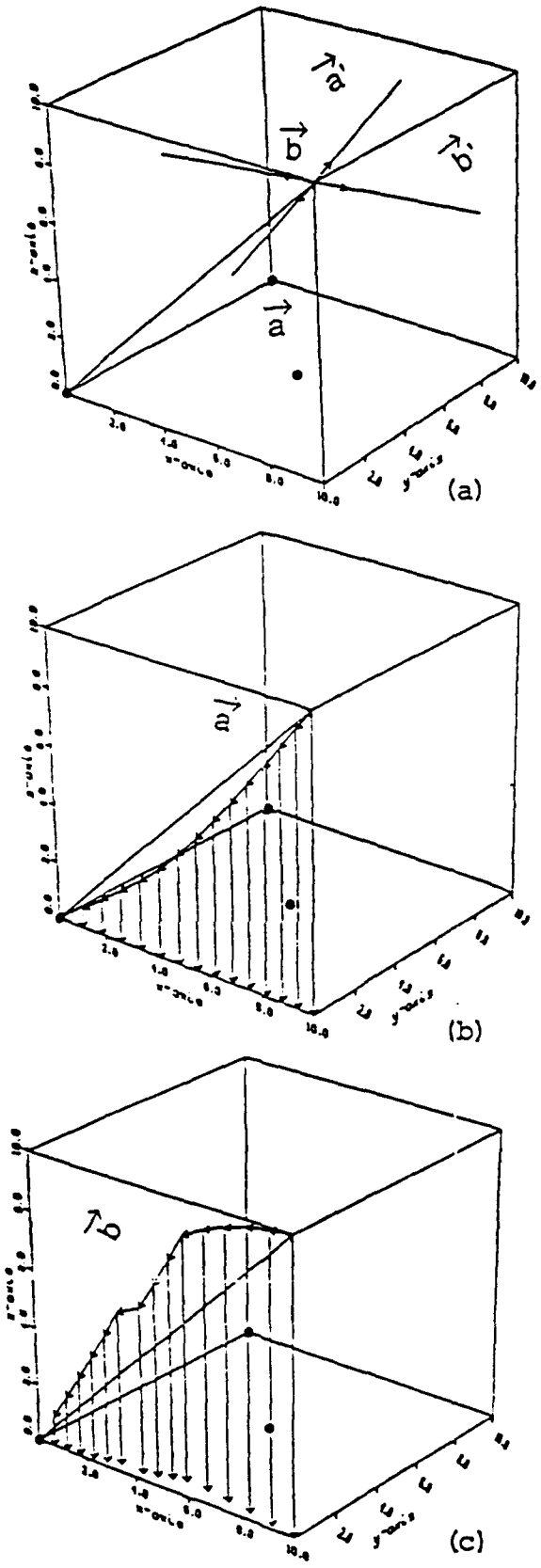

Figure A-10. Simulation of steering by gradiometer initial conditions with *derived vectors* $\vec{a}$, $\vec{b}$, $\vec{a}'$ and $\vec{b}'$ are shown in (a), and missile trajectories following vectors $\vec{a}$ and $\vec{b}$ are shown in (b) and (c). Magnetic dipoles of strengths K_1 = 1.0, K_2 = -0.1 and K_3 = 0.1 are assumed to be located at point (0,0,0), (0,10,0) and (5,5,0), respectively.

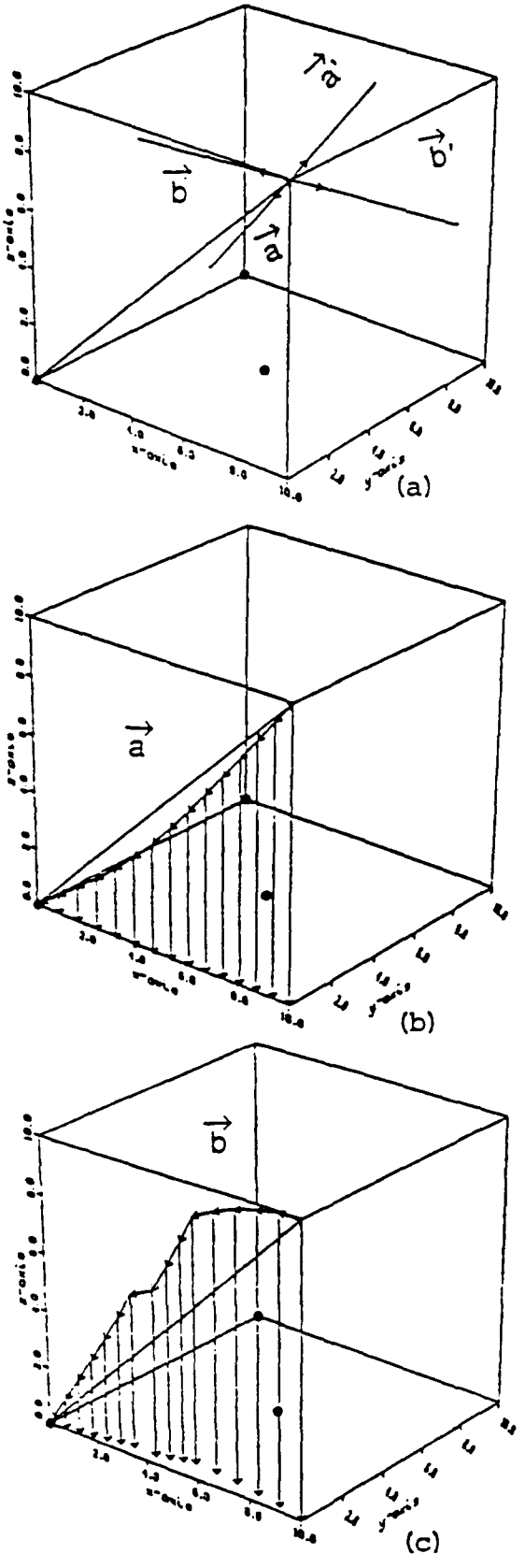

Figure A-11. Simulation of steering by gradiometer initial conditions with derived vectors $\vec{a}$, $\vec{b}$, $\vec{a}'$ and $\vec{b}'$ are shown in (a), and missile trajectories following vectors $\vec{a}$ and $\vec{b}$ are shown in (b) and (c). Magnetic dipoles of strengths K_1 = 1.0, K_2 = -0.2 and K_3 = 0.1 are assumed to be located at point (0,0,0), (0,10,0) and (5,5,0), respectively.

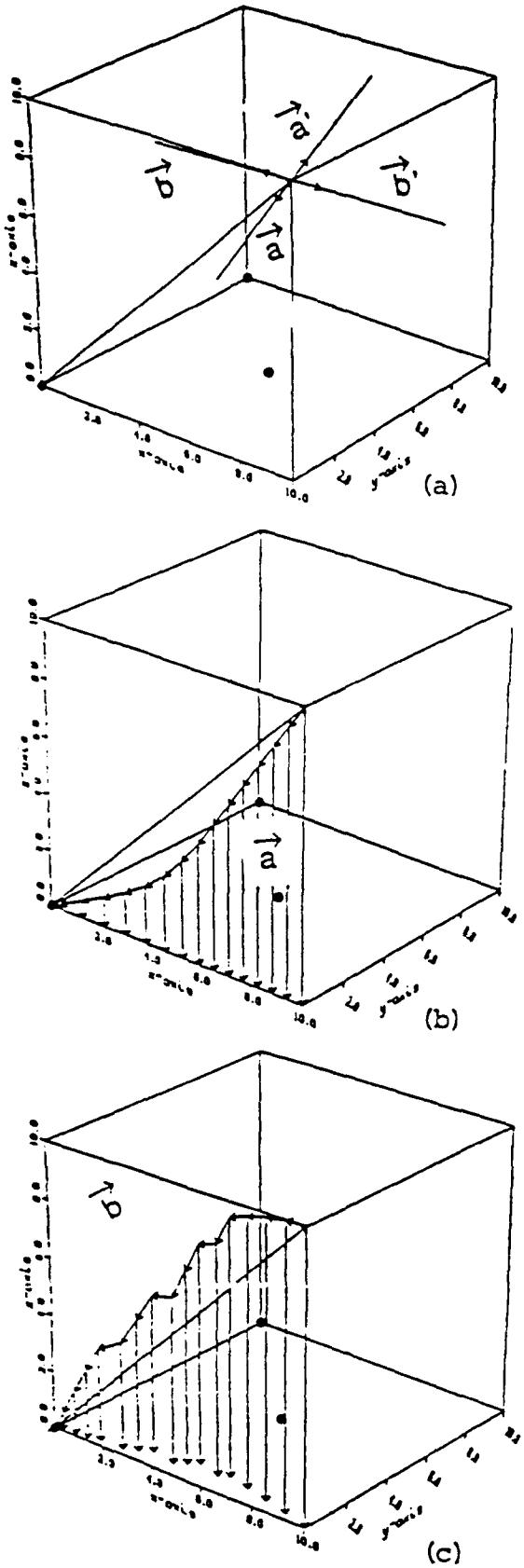

Figure A-12. Simulation of steering by gradiometer initial conditions with derived vectors $\vec{a}$, $\vec{b}$, $\vec{a}'$ and $\vec{b}'$ are shown in (a), and missile trajectories following vectors $\vec{a}$ and $\vec{b}$ are shown in (b) and (c). Magnetic dipoles of strengths $K_1 = 1.0$, $K_2 = 0.1$ and $K_3 = 0.2$ are assumed to be located at point (0,0,0), (0,10,0) and (5,5,0), respectively.

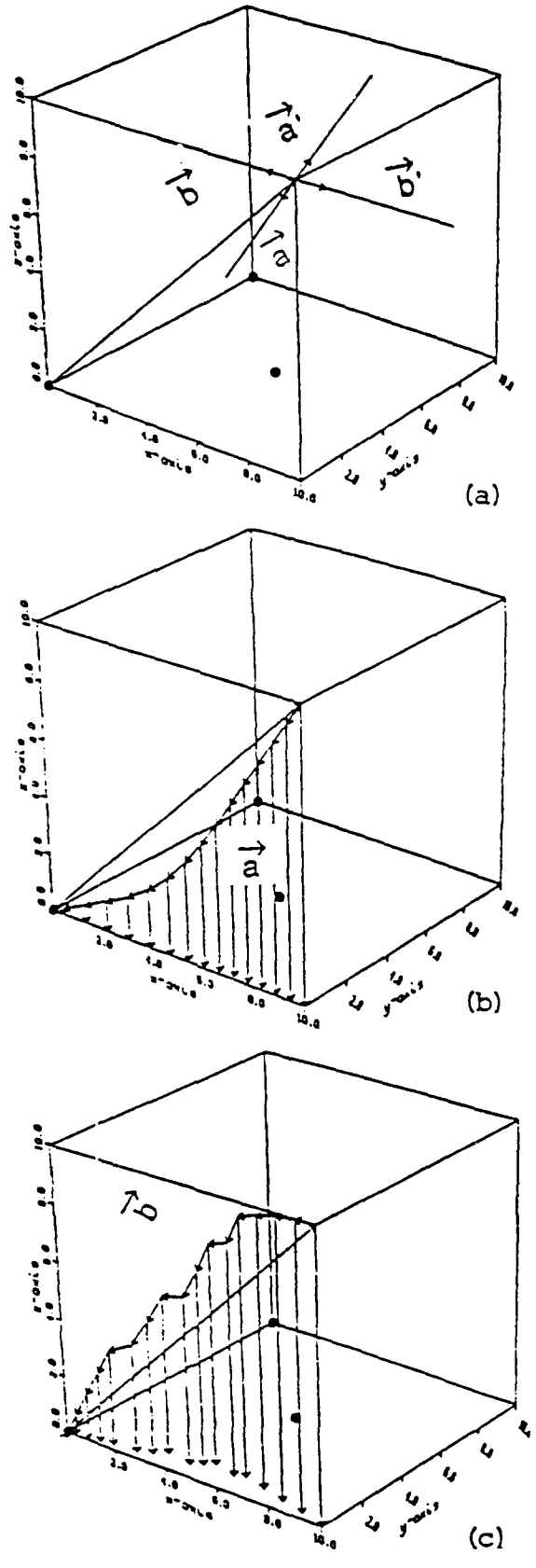

Figure A-13. Simulation of steering by gradiometer initial conditions with derived vectors $\vec{a}$, $\vec{b}$, $\vec{a}'$ and $\vec{b}'$ are shown in (a), and missile trajectories following vectors $\vec{a}$ and $\vec{b}$ are shown in (b) and (c). Magnetic dipoles of strengths $K_1 = 1.0$, $K_2 = 0.2$ and $K_3 = 0.2$ are assumed to be located at point (0,0,0), (0,10,0) and (5,5,0), respectively.

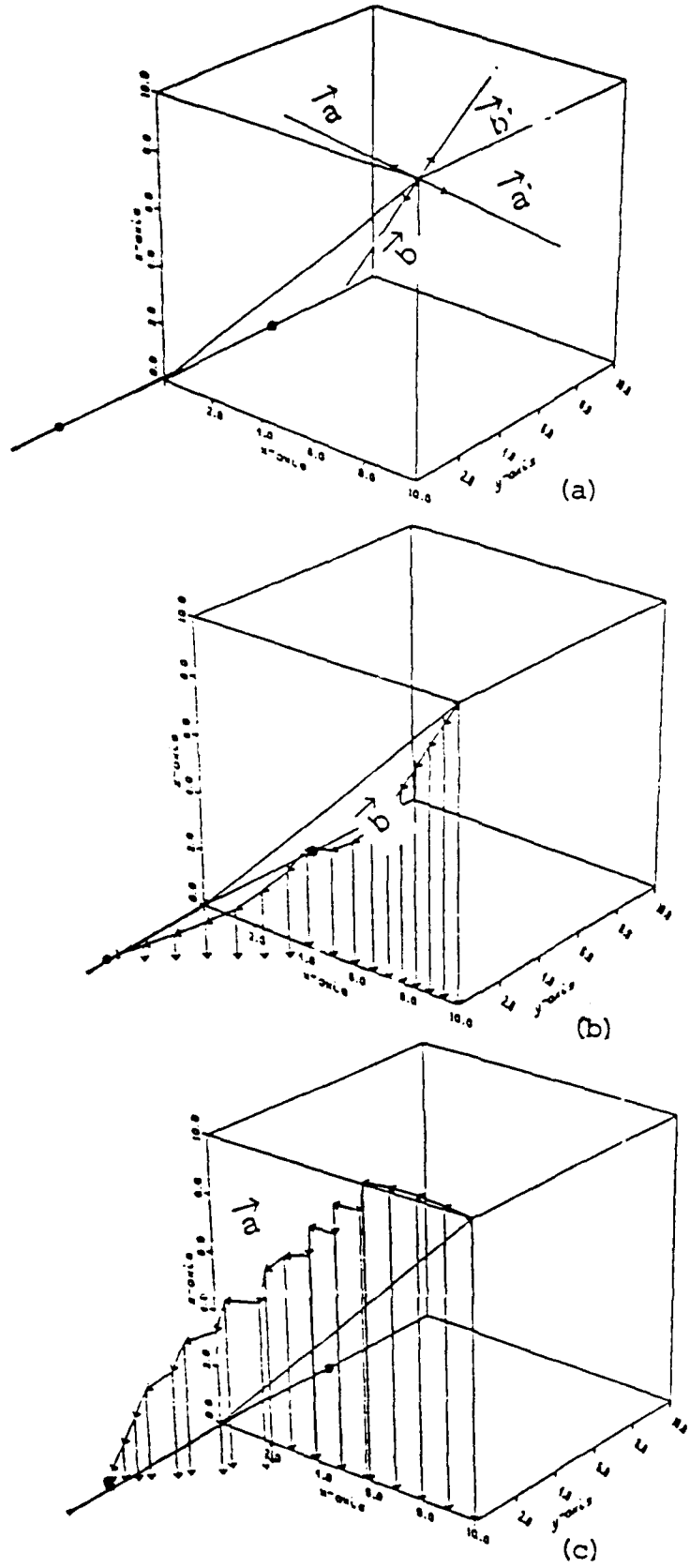

Figure A-14. Simulation of steering by gradiometer initial conditions with derived vectors $\vec{a}$, $\vec{b}$, $\vec{a}'$ and $\vec{b}'$ are shown in (a), and missile trajectories following vectors $\vec{a}$ and $\vec{b}$ are shown in (b) and (c). Magnetic dipoles of strengths K_1 = 1.0 and K_2 = 1.0 are assumed to be located at point (0,-5,0) and (0,5,0), respectively.

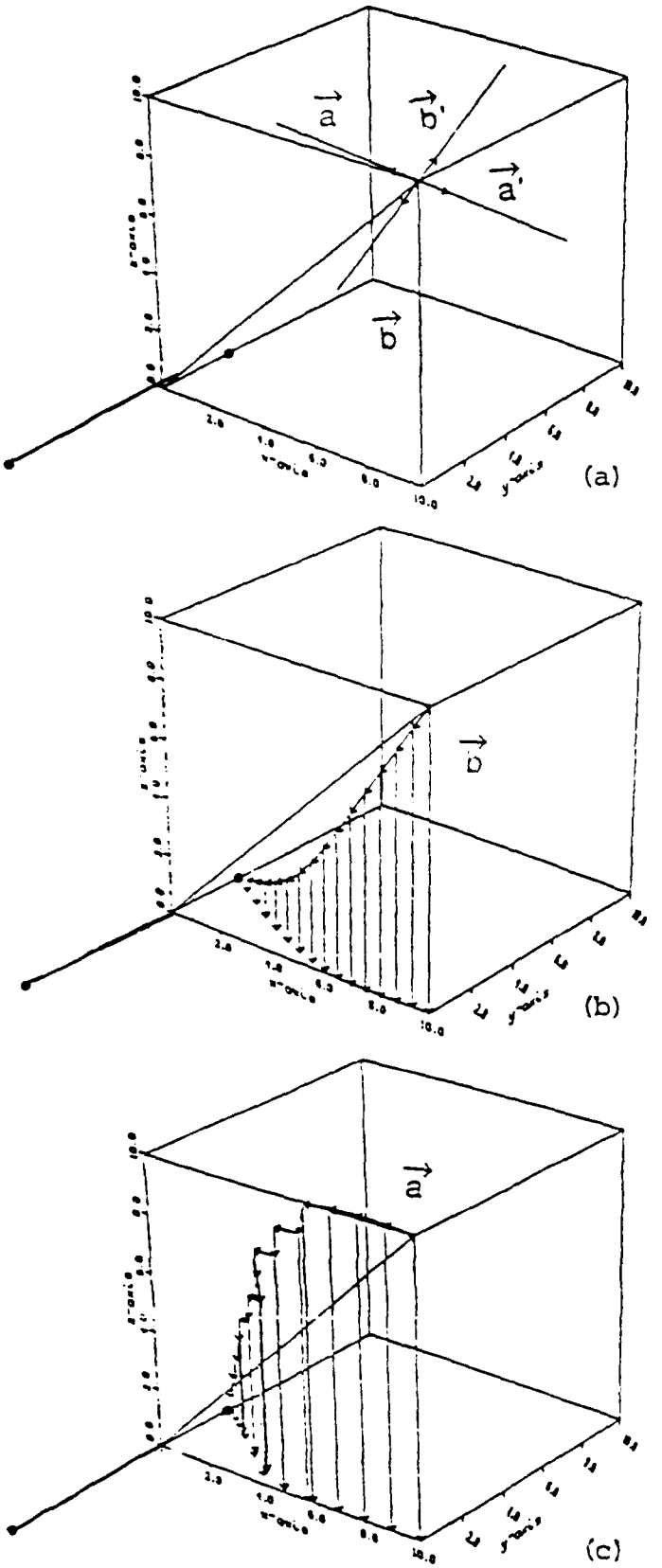

Figure A-15. Simulation of steering by gradiometer initial conditions with derived vectors $\vec{a}$, $\vec{b}$, $\vec{a}'$ and $\vec{b}'$ are shown in (a), and missile trajectories following vectors $\vec{a}$ and $\vec{b}$ are shown in (b) and (c). Magnetic dipoles of strengths $K_1 = 1.0$ and $K_2 = 0.2$ are assumed to be located at point (0,-7,0) and (0,3,0), respectively.